Check for updates

Interferon lambda restricts herpes simplex virus skin disease by suppressing neutrophil-mediated pathology

Drake T. Philip,[1] Nigel M. Goins,[1] Nicholas J. Catanzaro,[2] Ichiro Misumi,[3] Jason K. Whitmire,[1,3] Hannah M. Atkins,[4] Helen M. Lazear[1]

AUTHOR AFFILIATIONS See affiliation list on p. 25.

ABSTRACT Type III interferons (IFN-λ) are antiviral and immunomodulatory cytokines that have been best characterized in respiratory and gastrointestinal infections, but the effects of IFN-λ against skin infections have not been extensively investigated. We sought to define the skin-specific effects of IFN-λ against the highly prevalent human pathogen, herpes simplex virus (HSV). We infected mice lacking the IFN-λ receptor (*Ifnlr1*$^{-/-}$), both the IFN-λ and the IFN-α/β receptors (*Ifnar1*$^{-/-}$*Ifnlr1*$^{-/-}$), or IFN-λ cytokines (*Ifnl2/3*$^{-/-}$) and found that IFN-λ restricts the severity of HSV-1 and HSV-2 skin lesions without affecting viral loads. We used RNAseq to define IFN-λ- and IFN-β-induced transcriptional responses in primary mouse keratinocytes. Using conditional knockout mice, we found that IFN-λ signaling in both keratinocytes and neutrophils was necessary to control HSV-1 skin lesion severity and that IFN-λ signaling in keratinocytes suppressed CXCL9-mediated neutrophil recruitment to the skin. Furthermore, depleting neutrophils or blocking CXCL9 protected against severe HSV-1 skin lesions in *Ifnlr1*$^{-/-}$ mice. Altogether, our results suggest that IFN-λ plays an immunomodulatory role in the skin that restricts neutrophil-mediated pathology during HSV infection and suggests potential applications for IFN-λ in treating viral skin infections.

IMPORTANCE Type III interferons (IFN-λ) have been shown to have antiviral and immunomodulatory effects at epithelial barriers such as the respiratory and gastrointestinal tracts, but their effects on the skin have not been extensively investigated. We used mice lacking IFN-λ signaling to investigate the skin-specific effects of IFN-λ against the herpes simplex virus (HSV), which targets epithelial tissues to cause cold sores and genital herpes. We found that IFN-λ limited the severity of HSV skin lesions without affecting viral load and that this protective effect required IFN-λ signaling in both keratinocytes and neutrophils. We found that IFN-λ signaling in keratinocytes suppressed neutrophil recruitment to the skin and that depleting neutrophils protected against severe HSV skin lesions in the absence of IFN-λ. Altogether, our results suggest that IFN-λ plays an immunomodulatory role in the skin that restricts neutrophil-mediated pathology during HSV infection and suggests potential applications for IFN-λ in treating viral skin infections.

KEYWORDS herpes simplex virus, interferon lambda, skin, neutrophils, keratinocyte

The skin is one of the largest physical and immunologic barriers that separates the host from its environment and continuously encounters commensal and pathogenic microbes. Dysregulation of this barrier can result in inflammatory skin conditions, such as atopic dermatitis (eczema), or susceptibility to viral, bacterial, and fungal infections (1). Resident and infiltrating immune cells as well as barrier-specific cytokines contribute to providing a balanced immune response in the skin (2). The skin comprises two layers: the epidermis and dermis. The epidermis primarily consists of keratinocytes (skin epithelial cells) and T cells (CD8 and γδ). Keratinocytes form the physical barrier of the skin but also

are immunologically active, coordinating resident and infiltrating leukocyte responses (2). The dermis is primarily made of fibroblasts and is surveyed by a more diverse set of immune cells, including macrophages, dendritic cells, granulocytes, Langerhans cells, and T cells (CD8, CD4, and γδ) (2). Both layers of the skin act in concert to mediate immune responses, using a variety of cytokines and chemokines—including interferons (IFNs)—in balancing pathogen clearance with homeostasis and barrier integrity (3).

There are three families of IFNs: type I (IFN-α/β), type II (IFN-γ), and type III (IFN-λ), which are distinguished by their receptor usage (4). IFN-α/β and IFN-γ typically mediate systemic antiviral and immunomodulatory functions, whereas the activity of IFN-λ is most evident at epithelial barriers such as the respiratory and gastrointestinal tracts (5). There are four IFN-λ subtypes in humans (IFN-λ1–4), whereas mice express only IFN-λ2 and IFN-λ3 (5). All IFN-λ subtypes signal through the same heterodimeric receptor comprising the IFNLR1 and IL10Rβ subunits (6). IFN-λ intracellular signaling is similar to IFN-α/β in that upon receptor binding Jak1 and Tyk2 are activated to phosphorylate STAT1 and STAT2, which bind to IRF9 and translocate to the nucleus to drive IFN-stimulated gene (ISG) expression (6). Although IFN-λ and IFN-α/β canonically share the same intracellular signaling cascade and activate similar antiviral transcriptional programs, there has been a growing appreciation for their different antiviral and immunomodulatory functions. Their difference in function is due in part to kinetics, as IFN-α/β is induced more rapidly upon infection, whereas IFN-λ is produced later and for longer throughout infection (4, 5). Furthermore, whereas the IFN-α/β receptor (IFNAR1/IFNAR2 heterodimer) is expressed ubiquitously, IFNLR1 expression is restricted primarily to epithelial cells and select leukocytes such as neutrophils, dendritic cells, and macrophages (5). The high expression of IFNLR1 in epithelial tissues has led to substantial characterization of IFN-λ antiviral and immunomodulatory functions at epithelial barriers, including the respiratory tract and gastrointestinal tract. However, relatively little is known about the role of IFN-λ in the skin, even though the skin is an important epithelial barrier and home to a variety of IFN-λ-producing and responding cell types.

Therefore, we sought to investigate the functions of IFN-λ signaling in the skin using a highly prevalent human skin pathogen, herpes simplex virus (HSV-1 and HSV-2). HSV-1 primarily manifests as orofacial or genital lesions, but severe complications of HSV-1 infection include herpes encephalitis, herpes keratitis, and eczema herpeticum (7). HSV-2 most commonly causes genital herpes and can cause severe disease when transmitted to neonates at delivery (8). HSV-1 and HSV-2 establish life-long persistent (latent) infections in sensory neurons that are never cleared by the immune system; viral reactivation from latency results in recurrent epithelial lesions (cold sores and genital herpes) and transmission to new individuals. Over half of US adults are seropositive for HSV-1 and 15% are seropositive for HSV-2 (8). The disease associated with HSV-1 infection, in both mice and humans, is partly immune-mediated (7), but the viral and host factors that drive disease severity are not fully understood, including the effects of IFN-λ signaling in HSV-1 skin infection.

Here, we report a protective role of IFN-λ in restricting severe HSV-1 skin disease. Using a mouse model of HSV-1 skin infection, we found that IFN-λ-dependent protection from severe HSV-1 skin disease requires signaling in both keratinocytes and leukocytes (including neutrophils). We found that neutrophils are the primary leukocytes recruited to the skin during HSV-1 infection and that mice lacking IFN-λ signaling (*Ifnlr1*$^{-/-}$) have more skin-infiltrating neutrophils compared to wild-type mice. We found a greater proportion of neutrophils expressing a tissue homing integrin, leukocyte function-associated antigen-1 (LFA-1), in *Ifnlr1*$^{-/-}$ compared to wild-type mice, suggesting that *Ifnlr1*$^{-/-}$ neutrophils are highly recruited to and retained in HSV-1-infected skin. Furthermore, we showed that depleting neutrophils prevented the development of severe HSV-1 skin lesions in *Ifnlr1*$^{-/-}$ mice and that IFN-λ signaling in keratinocytes limits CXCL9-mediated neutrophil recruitment to the skin. Altogether, our results suggest that IFN-λ plays an immunomodulatory role in the skin that restricts neutrophil-mediated pathology

during HSV infection and suggests potential applications for IFN-λ in treating viral skin infections.

RESULTS

Defining HSV-1 skin lesion severity in the mouse flank infection model

Flank scarification is a well-established mouse model for studying HSV-1 pathogenesis (9–11). In the standard model, HSV-1 is scratched into depilated flank skin using a 27-gauge needle (9–11). The virus replicates at the inoculation site, infects innervating sensory neurons, and traffics in a retrograde direction to the neuron cell body located in the dorsal root ganglia (DRG), then traffics in an anterograde direction, returning to the entire dermatome innervated by that DRG, producing a dermatome skin lesion (Fig. S1A) (11). To improve the reproducibility of this infection model, we tested two modifications to the commonly used procedures. First, we depilated mice by manual plucking, rather than shaving plus chemical depilation (e.g., Nair cream). Plucking re-sets the hair growth cycle (3), producing an immunologically uniform environment across the depilated skin and is also faster and easier than shaving plus chemical depilation. We found no significant difference in dermatome lesion area for mice depilated by plucking compared to shaving plus Nair (Fig. S1B), suggesting that the method of depilation does not impact HSV-1 skin infection in this model, so for further experiments, we depilated mice by plucking. Next, we compared three methods for disrupting the skin barrier, as HSV-1 does not efficiently infect intact skin. We applied 10^6 focus-forming units (FFU) of HSV-1 (strain NS) onto depilated flank skin and abraded the inoculation site skin by (i) 40 gentle scratches with a 27G needle, (ii) 10 closely spaced punctures with a Quintip skin test (allergy needle), or (iii) a single puncture with a Greer pick skin test and measured viral loads in dermatome skin at 6 days post-infection (dpi). We found that skin viral loads corresponded to the extent of skin barrier disruption, with needle scarification producing a higher median viral load than a Quintip puncture (5.0 vs 4.2 Log_{10} FFU/g) and no virus detected after a Greer pick puncture (Fig. S1C). Although needle scarification produced higher median viral loads, there was a greater mouse-to-mouse variability compared to Quintip puncture [standard deviation (SD) 1.1 vs 0.7 Log_{10} FFU/g], and we and others have observed substantial operator-to-operator variability with needle scarification. Further, we found no difference in median lesion area between needle scarification and Quintip puncture (Fig. S1D); therefore, we used Quintip puncture to disrupt the skin barrier for further experiments.

We also sought to define a categorical system for classifying dermatome lesions as mild, moderate, or severe to better describe skin lesion phenotypes. We infected 20 wild-type mice with HSV-1, measured dermatome lesion area at 6 dpi, and found a mean area of 11 mm^2 (SD 12 mm^2) (Fig. S1E). We defined severe lesions as those with an area >1 SD above the mean (>23 mm^2), mild lesions as those with an area smaller than the average size of the inoculation site (<5 mm^2), and moderate lesions as 5–23 mm^2 (Fig. S1F and G). We used both lesion area and categorical severity to assess dermatome lesions in further experiments. Altogether, the flank infection model provides a robust system for assessing HSV-1 pathogenesis in the skin.

IFN-λ signaling protects mice from severe HSV skin disease

IFN-λ provides antiviral protection at epithelial barriers such as the respiratory and gastrointestinal tracts (12), but the effects of IFN-λ on viral infection in the skin have not been extensively investigated. To address this gap in the field, we infected wild-type mice and mice that lack the IFN-λ receptor ($Ifnlr1^{-/-}$) with 10^6 FFU of HSV-1 and evaluated skin lesion area, severity, and viral load 2–10 dpi (Fig. 1A through D). Experimental mice were generated by crossing mice with a floxed allele of the IFN-λ receptor ($Ifnlr1^{f/f}$) with mice hemizygous for Cre recombinase expression under a ubiquitous promoter (*ActB*-Cre), producing littermate Cre- (wild-type) and Cre+ ($Ifnlr1^{-/-}$) mice. Genotyping was performed retrospectively after data analysis, and experiments were conducted
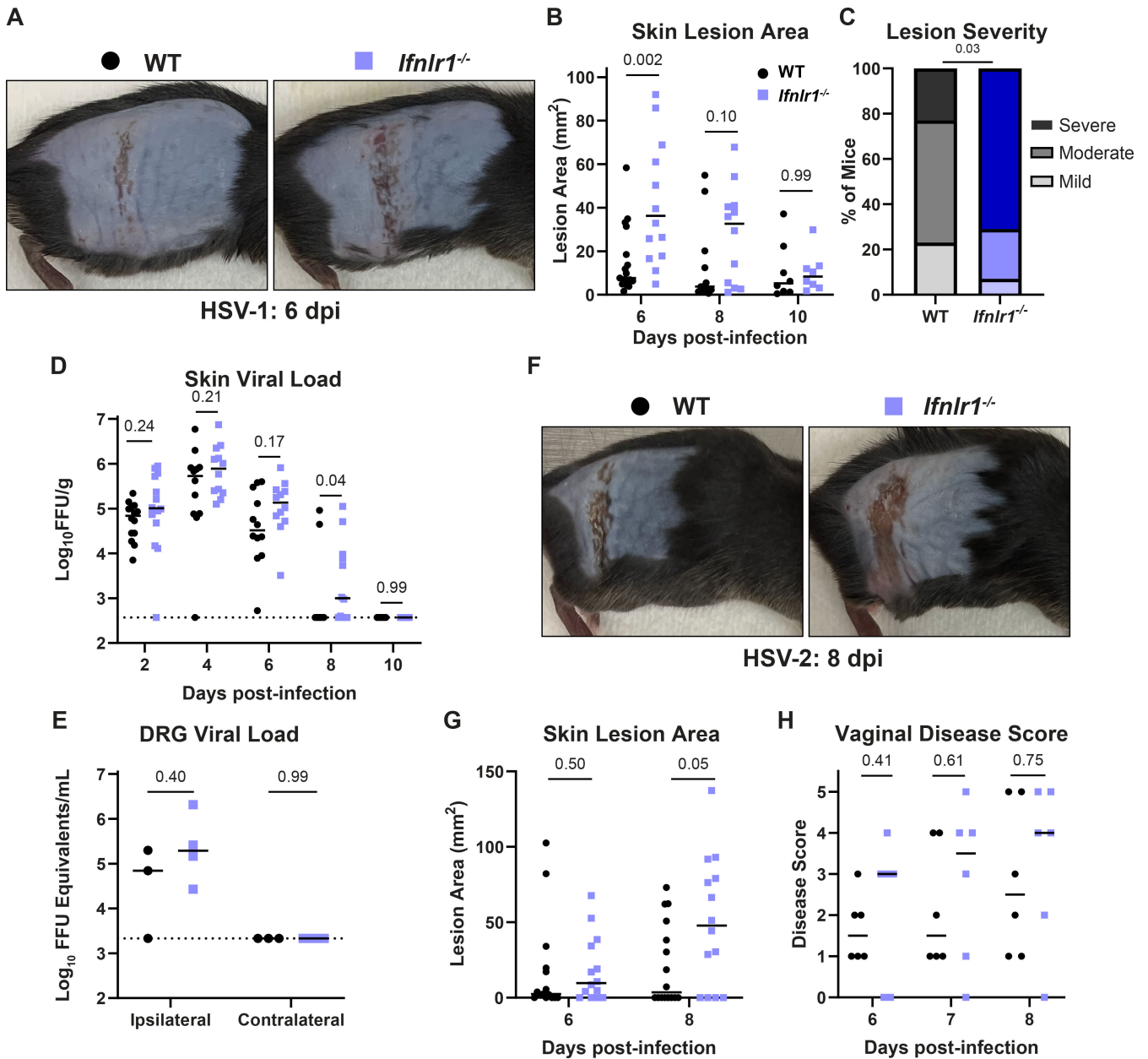
FIG 1 IFN-λ signaling protects against severe HSV skin disease without affecting viral replication. (A–E) Eight- to twelve-week-old male and female WT and *Ifnlr1*−/− mice were infected with 10^6 FFU of HSV-1 strain NS. (A) Dermatome skin lesions were photographed at 6 dpi. (B) HSV-1 skin lesions were measured from photographs at 6, 8, and 10 dpi using ImageJ. (C) Skin lesion severity was categorized based on the 6 dpi lesion area. (D) Skin viral loads were measured at 2–10 dpi by focus-forming assay. (E) Viral loads in ipsilateral and contralateral dorsal root ganglia (L2–L5 pooled for each mouse) were measured by qPCR. (F–G) Eight- to twelve-week-old male and female WT and *Ifnlr1*−/− mice were infected with 10^3 FFU of HSV-2 strain 333. (F) Dermatome lesions were photographed at 8 dpi. (G) HSV-2 skin lesions were measured from photographs at 6 and 8 dpi using ImageJ. (H) 8–12-week-old female WT and *Ifnlr1*−/− mice were infected with 10^3 FFU of HSV-2 strain 333 intravaginally and HSV-2 vaginal disease was scored at 6–8 dpi as follows: 1: mild redness and swelling, 2: visible ulceration and fur loss, 3: severe ulceration and signs of sickness, 4: hindlimb paralysis, and 5: moribund/dead. Differences in lesion area and viral load were compared by the Mann-Whitney *U* test. Differences in categorical skin disease were compared by the Cochran-Armitage test. *P* values are reported with *P* < 0.05 considered to be statistically significant. Data are combined from two to three independent experiments.

blinded to the *Ifnlr1* status of each mouse. We found that *Ifnlr1*−/− mice developed significantly larger skin lesions than wild-type mice at 6 dpi, the time of peak disease (median lesion area 36.2 vs 7.7 mm², *P* < 0.01; Fig. 1B), and that a greater proportion of *Ifnlr1*−/− mice developed severe skin lesions compared to wild-type mice (71% vs 23%,

$P < 0.05$; Fig. 1C). There was no significant difference in lesion area between $Ifnlr1^{-/-}$ and wild-type mice at 8 or 10 dpi (Fig. 1B). We measured viral loads by focus-forming assay from $Ifnlr1^{-/-}$ and wild-type skin lesions and from infected skin prior to lesion development (Fig. 1D). We found no significant differences in skin viral load between $Ifnlr1^{-/-}$ and wild-type mice at 2, 4, or 6 dpi, suggesting that IFN-λ signaling does not restrict HSV-1 replication in the skin. $Ifnlr1^{-/-}$ mice sustained viral loads in the skin longer than wild-type mice (8 of 12 $Ifnlr1^{-/-}$ mice positive at 8 dpi vs 2 of 12 wild-type mice, $P < 0.05$), but $Ifnlr1^{-/-}$ and wild-type mice both cleared the infection from the skin by 10 dpi (Fig. 1D). To determine whether differences in dermatome skin lesions resulted from differences in sensory neuron infection, we infected wild-type and $Ifnlr1^{-/-}$ mice, harvested DRG at 6 dpi, and quantified viral loads by qPCR. We found no significant differences in HSV-1 viral genomes in DRG at 6 dpi (Fig. 1E). Altogether, these results suggest that IFN-λ restricts HSV-1 skin lesion severity independently of a direct effect on viral replication.

We next tested whether IFN-λ had a similar protective effect against skin lesions caused by HSV-2. We infected mice with 1,000 FFU of HSV-2 (strain 333) and measured dermatome lesion areas at 6 and 8 dpi (Fig. 1F and G). The kinetics of HSV-2 infection were slower, with peak skin lesion area at 8 dpi, compared to 6 dpi for HSV-1, even though HSV-2 (333) was more virulent than HSV-1 (NS) [~75% mortality at an inoculation dose of 1,000 FFU of HSV-2 (333) compared to ~0% mortality at an inoculation dose of 10^6 FFU of HSV-1 (NS)]. Similar to HSV-1, $Ifnlr1^{-/-}$ mice developed significantly larger lesions compared to wild-type mice (median lesion area at 8 dpi 47.8 vs 3.6 mm^2, $P < 0.05$; Fig. 1G). Despite the slower kinetics of HSV-2 skin disease, the peak area of HSV-2 lesions in $Ifnlr1^{-/-}$ mice was larger than HSV-1 lesions (median lesion area 47.8 mm^2 at 8 dpi vs 36.2 mm^2 at 6 dpi; Fig. 1B and G). We next asked whether IFN-λ protected against HSV disease at other epithelial sites. Although both HSV-1 and HSV-2 infect the genital tract in humans and mice, HSV-1 does not cause overt vaginal disease in mice. Therefore, we used HSV-2 to assess the effects of IFN-λ during vaginal infection. We found no significant difference between $Ifnlr1^{-/-}$ and wild-type vaginal disease severity at 6–8 dpi (Fig. 1H). After 8 dpi, mice either began to recover or were euthanized due to neurologic disease signs (hindlimb paralysis and hunching). Altogether, these results show that IFN-λ protects against severe skin disease caused by both HSV-1 and HSV-2.

The protective effect of IFN-λ in the skin does not require IFN-α/β signaling

IFN-λ and IFN-α/β signal through distinct receptors but canonically activate an overlapping JAK/STAT signaling cascade and transcriptional response (6). To determine whether the protective effects of IFN-λ in the skin acted via cross-talk with IFN-α/β signaling, we infected mice lacking the IFN-α/β receptor ($Ifnar1^{-/-}$) or both the IFN-α/β and IFN-λ receptors ($Ifnar1^{-/-}$ $Ifnlr1^{-/-}$ double-knockout, DKO) with HSV-1 and evaluated survival, skin lesion area and severity, and viral loads (Fig. 2A through E). As expected, in the absence of IFN-α/β signaling, the kinetics of HSV-1 infection were faster and the disease was more severe, with all mice succumbing at 5–8 dpi (Fig. 2A). At 4 dpi, the first day mice developed lesions, $Ifnar1^{-/-}$ $Ifnlr1^{-/-}$ DKO mice developed significantly larger skin lesions compared to $Ifnar1^{-/-}$ mice (median lesion area 67.8 vs 19.7 mm^2, $P < 0.001$; Fig. 2B and C) and a significantly larger proportion developed severe lesions (100% vs 44%, $P < 0.01$; Fig. 2D). We found no significant difference in skin viral loads at 2 or 4 dpi (Fig. 2E). Altogether, these data indicate that IFN-λ limits severe HSV-1 skin disease independently of IFN-α/β and independent of a direct antiviral effect on HSV-1 replication in the skin.

IFN-λ cytokines protect against severe HSV-1 skin disease

To determine whether mice lacking IFN-λ cytokines recapitulate the phenotype of mice lacking the IFN-λ receptor, we infected mice lacking IFN-λ2 and IFN-λ3 ($Ifnl2/3^{-/-}$), the only IFN-λ cytokines produced in mice (13), and measured skin lesion area, disease severity, and skin viral loads (Fig. 3A through D). At 6 dpi, $Ifnl2/3^{-/-}$ mice developed significantly larger skin lesions compared to wild-type mice (median area 20.2 vs 7.1
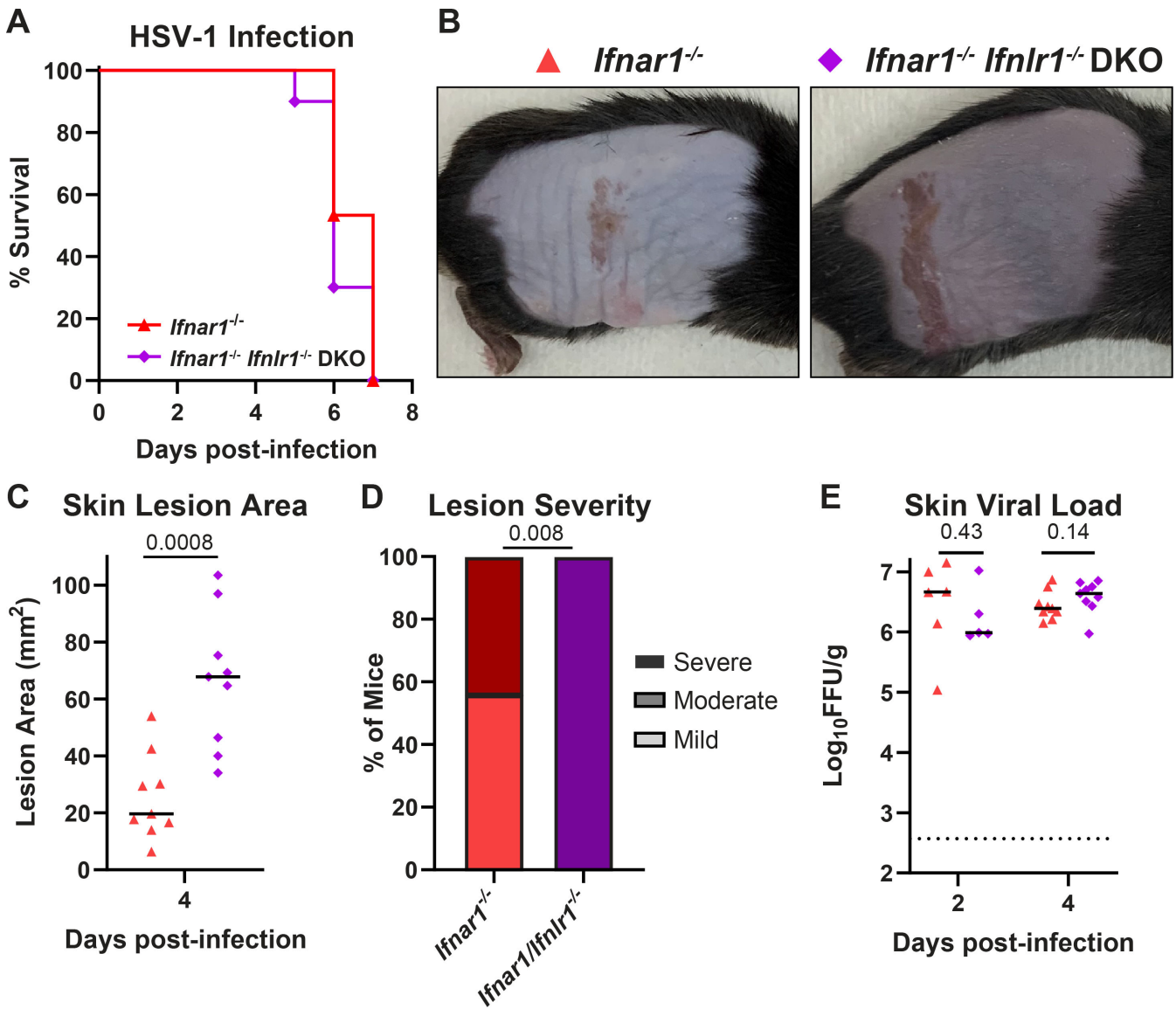
FIG 2 The protective effect of IFN-λ in the skin does not require IFN-α/β signaling. Eight- to twelve-week-old *Ifnar1*^{−/−} and *Ifnar1*^{−/−} *Ifnlr1*^{−/−} DKO male and female mice were infected with 10^6 FFU of HSV-1. (A) Lethality was monitored daily (n = 15 *Ifnar1*^{−/−} and n = 10 DKO mice). (B) Dermatome skin lesions were photographed at 4 dpi. (C) Skin lesion areas were measured from photographs at 4 dpi using ImageJ. (D) Skin lesion severity was categorized based on the 4-dpi lesion area. (E) Skin viral loads were measured at 2 and 4 dpi by focus-forming assay. Survival differences were compared by the Mantel-Cox Log-Rank test. Differences in lesion area and viral load were compared by the Mann-Whitney *U* test, and differences in categorical skin disease were compared by the Cochran-Armitage test. *P* values are reported with *P* < 0.05 considered to be statistically significant. Data are combined from three independent experiments.

mm², *P* < 0.01; Fig. 3B), and a significantly higher proportion of *Ifnl2/3*[−/−] mice developed severe skin lesions compared to wild-type mice (45% vs 15%, *P* < 0.01, Fig. 3C) with no significant difference in skin viral loads (Fig. 3D). Altogether, the phenotype of mice lacking IFN-λ cytokines was consistent with the phenotype of mice lacking the IFN-λ receptor, providing an independent line of evidence that IFN-λ signaling restricts severe HSV-1 skin disease.

Although some type I IFNs, such as IFN-α and IFN-β, can be produced by many cell types, IFN-κ is a type I IFN that is thought to be produced predominantly by keratinocytes (14, 15). To determine whether a keratinocyte-specific type I IFN might play a role in controlling skin disease caused by HSV-1, we infected *Ifnk*^{−/−} mice. We found no significant differences in lesion area, disease severity, or skin viral loads between *Ifnk*^{−/−} mice
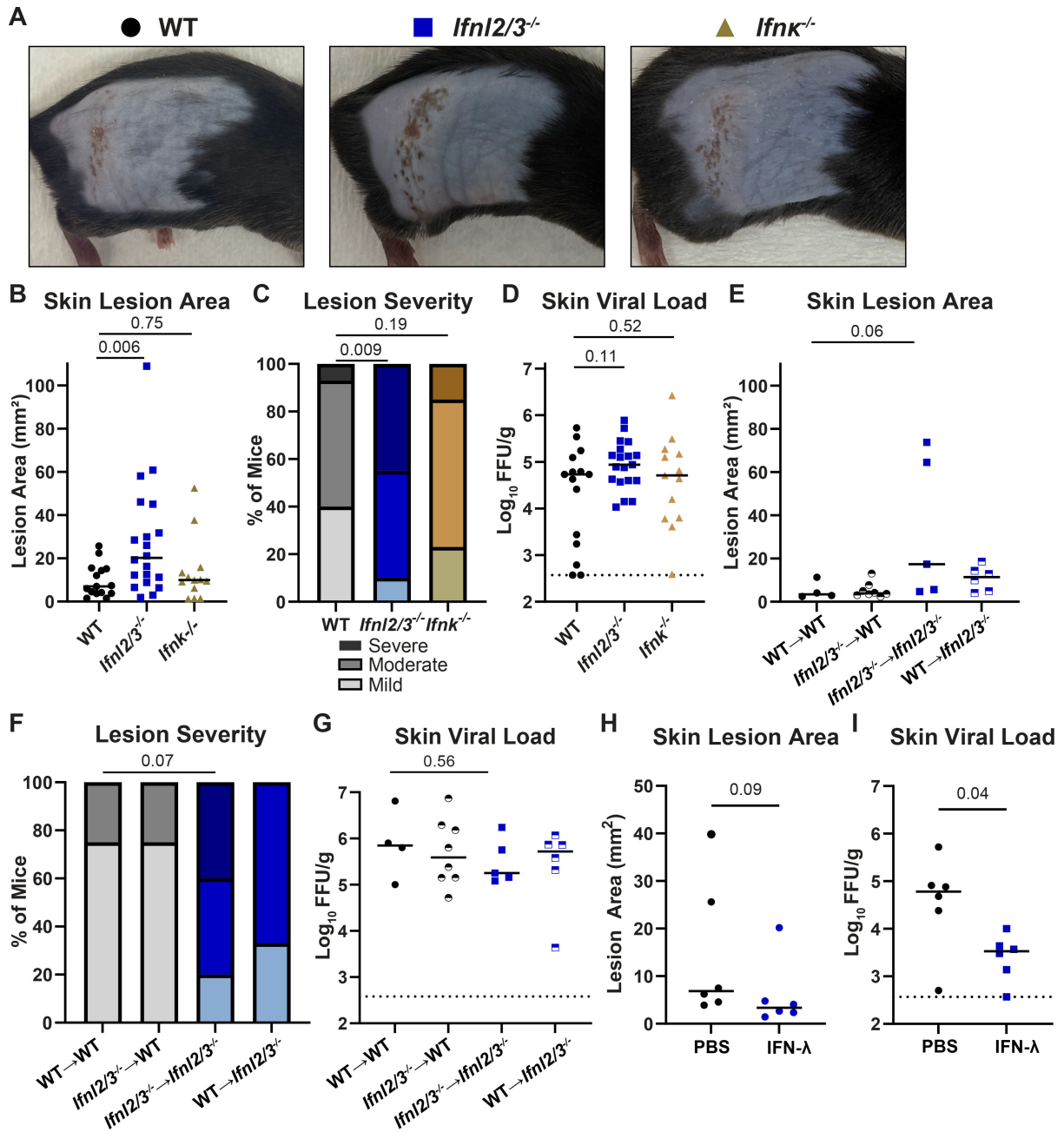
FIG 3 IFN-λ cytokines protect against severe HSV-1 skin disease. (A–D) Eight- to twelve-week-old WT, *Ifnl2/3*$^{-/-}$, and *Ifnk*$^{-/-}$ male and female mice were infected with 10^6 FFU of HSV-1. (A) Dermatome skin lesions were photographed at 6 dpi. (B) Skin lesion areas were measured from photographs at 6 dpi using ImageJ. (C) Skin lesion severity was categorized based on the 6 dpi lesion area. (D) Skin viral loads were measured at 6 dpi by FFA. (E–G) Eight-week-old WT and *Ifnl2/3*$^{-/-}$ male and female mice were lethally irradiated and transfused with 10^7 bone marrow cells from WT or *Ifnl2/3*$^{-/-}$ donors. Ten weeks later, mice were infected with 10^6 FFU of HSV-1. (E) Skin lesion areas were measured from photographs at 6 dpi using ImageJ. (F) Skin lesion severity was categorized based on the 6 dpi lesion area. (G) Skin viral loads were measured at 6 dpi by FFA. (H–I) Eight- to twelve-week-old WT male and female mice were depilated and then topically treated with 5 µg of recombinant murine IFN-λ3 or PBS. Twenty-four hours later, mice were infected with 10^6 FFU of HSV-1 at the treated site. (H) Skin lesion areas were measured from photographs at 6 dpi using ImageJ. (I) Skin viral loads were measured at 6 dpi by FFA. Differences in lesion area and viral load were compared by the Mann-Whitney *U* test, and differences in categorical skin disease were compared by the Cochran-Armitage test. *P* values are reported with $P < 0.05$ considered to be statistically significant. Data are combined from two to three independent experiments.

and wild-type mice (Fig. 3A through D), suggesting that, despite its keratinocyte-specific nature, IFN-κ does not play a key role in controlling HSV-1 infection in the skin.

To determine the source of protective IFN-λ during HSV-1 skin infection, we used bone marrow chimeras between wild-type and *Ifnl2/3* $^{-/-}$ mice, generating mice that lacked the ability to produce IFN-λ2/3 in either their hematopoietic or stromal compartments. Due to a lack of antibodies to detect IFN-λ, we used PCR genotyping to confirm effective bone marrow engraftment in recipients. We then infected IFN-λ chimeric mice with HSV-1 and evaluated skin disease at 6 dpi (Fig. 3E and F). *Ifnl2/3*$^{-/-}$ mice receiving *Ifnl2/3*$^{-/-}$ bone marrow showed a trend toward larger lesions and more severe disease than wild-type mice receiving wild-type bone marrow (median area 17.3 vs 3.5 mm^2, P = 0.06; Fig. 3E), consistent with our observations in non-irradiated mice. However, we found that mice retaining IFN-λ production in either their hematopoietic compartment or their stromal compartment were protected from severe HSV-1 skin disease, suggesting that multiple cell types can produce protective IFN-λ during HSV-1 skin infection. As in our previous experiments, the effects of IFN-λ on skin lesion severity were independent of an effect on viral load (Fig. 3G).

Exogenous IFN-λ treatment has shown therapeutic potential against various viral infections and autoimmune diseases (16–20); therefore, we sought to determine whether topical administration of IFN-λ could limit HSV-1 infection and skin lesions. We depilated mice 2 days prior to infection, pretreated topically with 5 µg of IFN-λ, and infected with HSV-1 on the treated site 1 day later. We found a modest decrease in lesion areas in IFN-λ-pretreated mice at 6 dpi compared to phosphate-buffered saline (PBS)-pretreated mice (median area 3.4 vs 6.9 mm^2, P = 0.09; Fig. 3G). Additionally, we found that viral loads at 6 dpi were significantly reduced in IFN-λ-pretreated mice compared to PBS-pretreated mice (median viral load 3.53 Log$_{10}$ FFU/g vs 4.78 Log$_{10}$ FFU/g, P < 0.05; Fig. 3H). Altogether, these data indicate that prophylactic administration of exogenous IFN-λ can limit severe HSV-1 skin disease, suggesting potential opportunities for therapeutic interventions.

IFN-λ signaling in both keratinocytes and leukocytes is necessary to restrict severe HSV-1 skin disease

The skin comprises diverse cell types, including keratinocytes and resident and infiltrating leukocytes. To determine which IFN-λ responsive cell types contribute to controlling HSV-1 skin infection, we used conditional knockout mice lacking IFN-λ signaling in keratinocytes (*K14*-Cre-*Ifnlr1*$^{-/-}$) or leukocytes (*Vav*-Cre-*Ifnlr1*$^{-/-}$). These mice were bred as Cre hemizygotes, generating littermate Cre− controls (wild-type), and were genotyped retrospectively, allowing experiments to be performed blinded to the *Ifnlr1* status of each mouse. *Vav*-Cre-*Ifnlr1*$^{-/-}$ mice have been previously reported (21, 22); however, to our knowledge, this is the first derivation of *K14*-Cre-*Ifnlr1*$^{-/-}$ mice. To validate the conditional depletion of the *Ifnlr1* in these mice, we used PCR genotyping in specific tissues in wild-type (Cre−) and *K14*-Cre-*Ifnlr1*$^{-/-}$ (Cre+) mice and found Cre-mediated rearrangement of the *Ifnlr1*$^{f/f}$ allele only in epithelial tissues (Fig. S2). Conditional knockout mice were compared to *Ifnlr1*$^{-/-}$ mice generated by crossing *Ifnlr1*$^{f/f}$ mice to mice expressing Cre recombinase under a CMV promoter and subsequently bred as knockout × knockout.

We infected wild-type, *Ifnlr1*$^{-/-}$, *K14*-Cre-*Ifnlr1*$^{-/-}$, and *Vav*-Cre-*Ifnlr1*$^{-/-}$ mice with HSV-1 and evaluated skin lesion area, disease severity, and viral loads at 6 dpi (Fig. 4A through D). We found that *Ifnlr1*$^{-/-}$ mice developed significantly larger lesions than wild-type mice (median area 13.1 vs 6.7 mm^2, P < 0.01) (Fig. 4B) and a greater proportion of these mice developed severe skin disease (34% vs 14%, P < 0.01) (Fig. 4C), further supporting a role for IFN-λ in controlling severe HSV-1 skin disease in an independent line of *Ifnlr1*$^{-/-}$ mice compared to those used in our earlier experiments (Fig. 1). We found that mice lacking IFN-λ signaling exclusively in keratinocytes or leukocytes developed skin lesions similar in size to *Ifnlr1*$^{-/-}$ mice (median area 15.7, 14.6, and 13.1 mm^2, P > 0.05) (Fig. 4C) and a similar proportion developed severe lesions (40%, 44%, and 34%, P > 0.05) (Fig. 4D). We found no significant differences in skin viral loads comparing *Ifnlr1*$^{-/-}$ mice to wild-type or comparing conditional knockouts to *Ifnlr1*$^{-/-}$ (Fig. 4D). Altogether, these data indicate
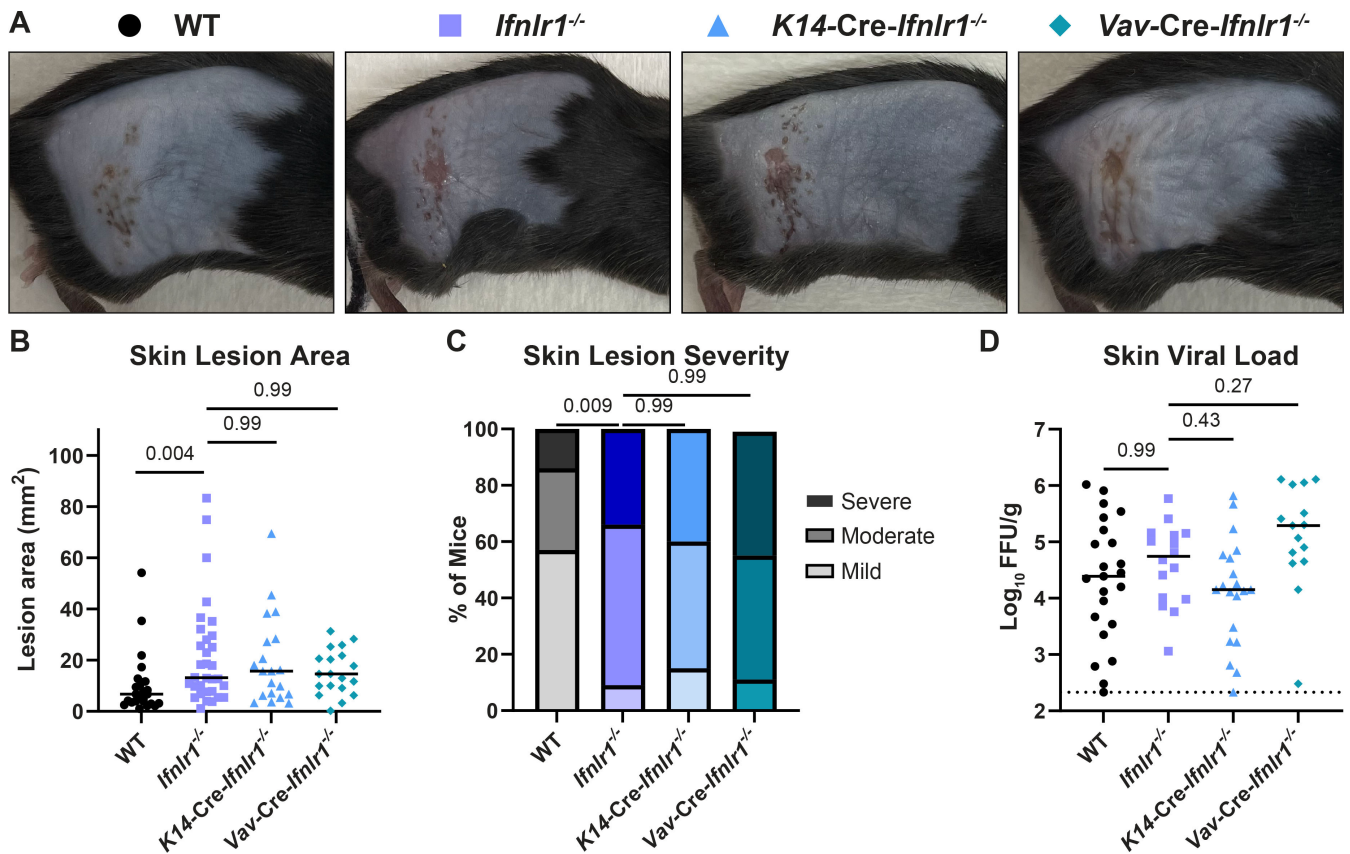
FIG 4 IFN-λ signaling in both keratinocytes and leukocytes is necessary to restrict severe HSV-1 skin disease. Eight- to twelve-week-old male and female WT, *Ifnlr1*$^{-/-}$, *K14*-Cre-*Ifnlr1*$^{-/-}$, and *Vav*-Cre-*Ifnlr1*$^{-/-}$ mice were infected with 10^6 FFU of HSV-1. (A) Dermatome skin lesions were photographed at 6 dpi. (B) Skin lesion areas were measured from photographs at 6 dpi using ImageJ. (C) Skin lesion severity was categorized based on the 6 dpi lesion area. (D) Skin viral loads were measured at 6 dpi by FFA. Differences in lesion area and viral load were compared by the Mann-Whitney U test, and differences in categorical skin disease were compared by the Cochran-Armitage test. P values are reported with $P < 0.05$ considered to be statistically significant. Data are combined from four independent experiments for *K14*-Cre-*Ifnlr1*$^{-/-}$ mice and ~10 independent experiments for WT, *Ifnlr1*$^{-/-}$, and *Vav*-Cre-*Ifnlr1*$^{-/-}$ mice.

that IFN-λ signaling in both keratinocytes and leukocytes is necessary to control severe HSV-1 skin disease.

IFN-λ signaling in keratinocytes differentially regulates inflammatory genes, including CXCL9

Because we found that IFN-λ signaling in both keratinocytes and leukocytes was necessary to control HSV-1 skin lesion severity, we next asked whether this was due to cross-talk between keratinocytes and leukocytes. To understand how IFN-λ could be mediating signaling between epithelial cells and immune cells, we first generated IFN receptor knockout A549 cells, a human lung epithelial cell line. We treated *IFNLR1* KO, *IFNAR1* KO, or nontargeting control (RenLuc) A549 cells with recombinant IFN-β or IFN-λ and measured the induction of the ISG *IFIT1* by RT-qPCR. As expected, *IFNLR1* KO cells responded to IFN-β but not IFN-λ and *IFNAR1* KO cells responded to IFN-λ but not IFN-β (Fig. S3A). We then treated control and IFN receptor KO cells with 50 ng/mL IFN-λ, 5 ng/mL IFN-β, or media alone for 8 hours and performed bulk RNAseq (Fig. S3B through F). We found that the transcriptional response after IFN-λ treatment in A549 cells was modest compared to IFN-β (Table S1), consistent with prior studies (23, 24). However, prior studies that used primary cells rather than cell lines found more robust transcriptional responses induced by IFN-λ (25–28). We therefore investigated IFN-λ-induced transcriptional responses in primary keratinocytes.

To define the IFN-λ-specific response in keratinocytes and understand how IFN-λ could be signaling through keratinocytes to mediate their cross talk with leukocytes, we generated primary keratinocytes from wild-type, *Ifnar1*$^{-/-}$, *Ifnlr1*$^{-/-}$, and *Ifnar1*$^{-/-}$*Ifnlr1*$^{-/-}$ DKO mice and treated them with 5 ng of IFN-λ, 5 ng of IFN-β, or media for 24 hours. We first measured the induction of *Ifit1* by RT-qPCR. As expected, IFN-β did not induce a response in *Ifnar1*$^{-/-}$ cells, IFN-λ did not induce a response in *Ifnlr1*$^{-/-}$ cells, and neither IFN induced a response in *Ifnar1*$^{-/-}$*Ifnlr1*$^{-/-}$ cells (Fig. 5A). We then performed bulk RNAseq with the goal of identifying IFN-λ-specific antiviral immune response genes. By principal component analysis, triplicate samples clustered together, but genotypes were distinct even without IFN treatment, suggesting differences in tonic IFN signaling in keratinocytes (Fig. 5B). While the IFN-β response was largely unchanged in *Ifnlr1*$^{-/-}$ cells compared to wild type, the IFN-λ response was diminished in *Ifnar1*$^{-/-}$ cells by both RT-qPCR (Fig. 5A) and principal component analysis (Fig. 5B), suggesting cross talk between IFN-λ and IFN-β signaling in keratinocytes as well as in A549 cells (Fig. S3B). Although the IFN-λ response generally is reported to be less potent than the IFN-α/β response (Fig. S3) (5), we found that many ISGs (including *Ifit1* and *Rsad2*) were induced to a similar magnitude by IFN-λ and IFN-β (Fig. 5A and C). We found a subset of ISGs in primary keratinocytes to be differentially induced by IFN-λ but not IFN-β (Fig. 5D). However, upon inspecting the IFN-λ-specific gene list, we found that while 11 or 10 genes did meet our differential threshold [two-fold change, false discovery rate (FDR) *P* < 0.05], these genes all were induced to a similar extent by IFN-β (although not quite reaching the differential threshold) (Fig. 5E). Moreover, none of the genes identified as IFN-λ specific in wild-type or knockout keratinocytes overlapped (Table S2), arguing against a set of ISGs that are induced in an IFN-λ-specific manner in this system.

We next analyzed the IFN-λ response relative to the IFN-β response in WT and knockout keratinocytes to identify genes that are differentially regulated by IFN-λ compared to IFN-β (Fig. 5F). We found that the chemokine CXCL9 was one of the top differentially regulated genes between IFN-λ and IFN-β treatment in both wild-type and the corresponding receptor knockout keratinocytes. Notably, *Cxcl9* was significantly less induced after IFN-λ treatment compared to IFN-β in wild-type keratinocytes (9.7-fold vs 65.0-fold) and knockout keratinocytes (23.0-fold vs 58.5-fold). Because CXCL9 is known to recruit a variety of immune cells such as T cells, NK cells, and neutrophils (29–31), we next sought to characterize IFN-λ-dependent leukocyte changes in HSV-1-infected skin to identify possible players in IFN-λ-mediated protection by keratinocytes and leukocytes.

Skin lesions in *Ifnlr1*$^{-/-}$ mice exhibit extensive neutrophil infiltration and severe pathology

To define IFN-λ-dependent changes in leukocyte populations in response to HSV-1 infection, we harvested skin lesions and adjacent healthy skin from *Ifnlr1*$^{-/-}$ and wild-type mice at 6 dpi and analyzed leukocyte populations by flow cytometry. We found no significant difference between *Ifnlr1*$^{-/-}$ and wild-type leukocyte population frequencies or numbers in healthy skin at 6 dpi (Fig. S4A and B). Furthermore, we found no differences in leukocyte frequency or numbers, including dendritic cells, macrophages, CD4 and CD8 T cells, B cells, or NK cells, between *Ifnlr1*$^{-/-}$ and wild-type skin lesions at 6 dpi (Fig. S4A and B). However, we found that skin lesions from *Ifnlr1*$^{-/-}$ mice exhibited a significantly higher frequency of neutrophils (%CD45+ CD11b+ Ly6 G^{hi}, Fig. 6A; Fig. S5) compared to wild-type mice at 6 dpi (mean neutrophil frequency 21.1% vs 6.7%; Fig. 6B). Of note, we did not find significant differences in the absolute number of neutrophils between wild-type and *Ifnlr1*$^{-/-}$ skin lesions, likely due to increased variance in these data without normalization to total cell numbers (Fig. S4C). Although we found a significant increase in γδT cells between *Ifnlr1*$^{-/-}$ and wild-type mice (Fig. S4A), we did not further investigate these cells as they are not known to be IFN-λ responsive and are less abundant in the skin compared to neutrophils. This increase in neutrophil frequency was specific to the skin lesion because in adjacent healthy skin, neutrophil abundance was very low and there was no significant difference between *Ifnlr1*$^{-/-}$ and wild-type mice
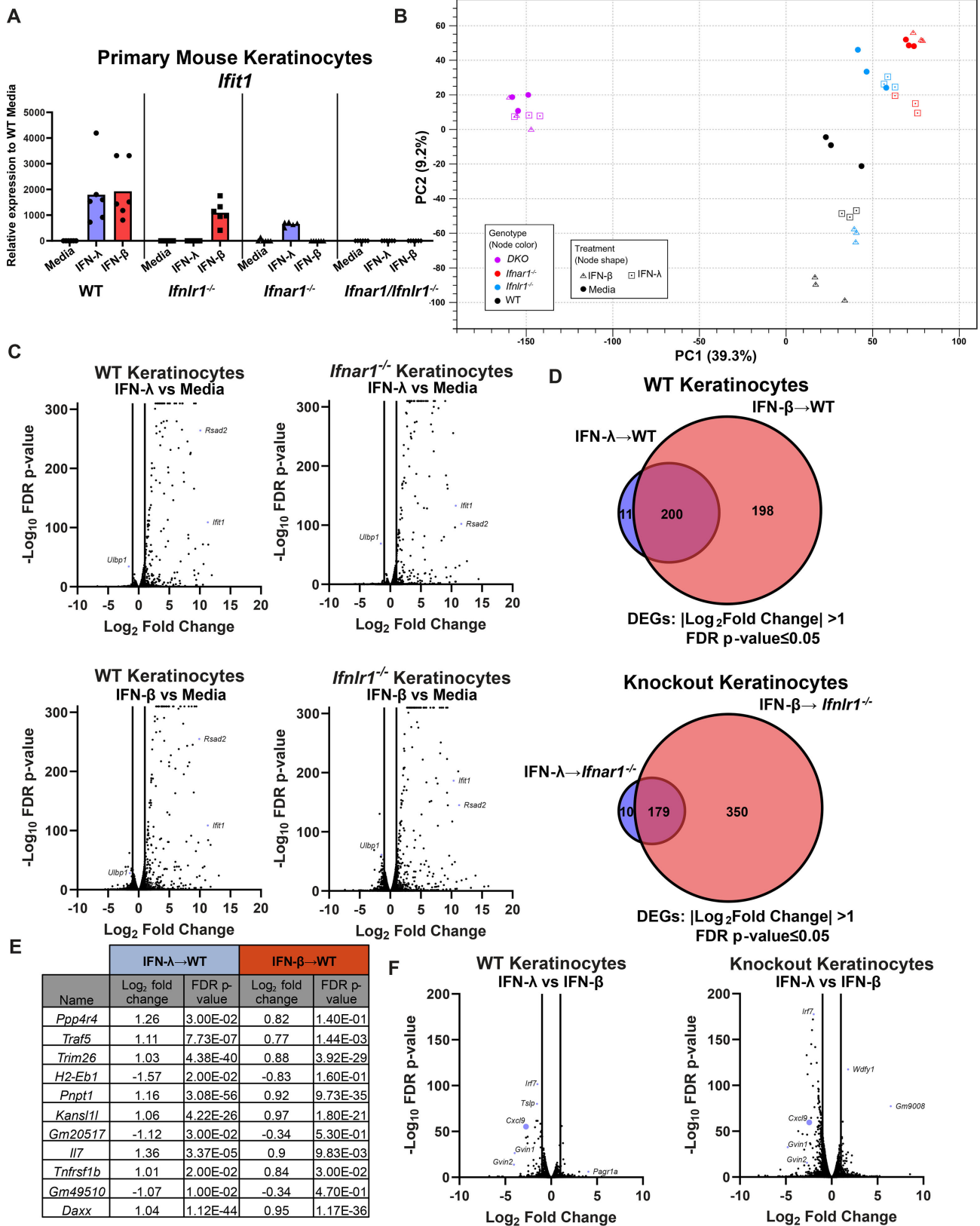
FIG 5 IFN-λ signaling in keratinocytes differentially regulates CXCL9 induction. Primary keratinocytes were prepared from WT, *Ifnlr1*$^{-/-}$, *Ifnar1*$^{-/-}$, and *Ifnar1*$^{-/-}$*Ifnlr1*$^{-/-}$ DKO mice and treated with IFN-λ3 (5 ng/mL), IFN-β (5 ng/mL), or media alone for 24 hours. (A) RNA was extracted, and IFN-stimulated gene expression was measured by RT-qPCR. *Ifit1* expression is shown relative to *ActB* (housekeeping gene) and normalized to expression in media-treated WT cells. Results (Continued on next page)

FIG 5 (Continued)

represent six samples from two independent experiments. (B–F) RNA from three samples per genotype per treatment was analyzed by RNAseq. (B) Principal component analysis for all analyzed samples. (C) Volcano plots showing differentially expressed genes (DEGs) after IFN-λ or IFN-β treatment, compared to media-only treated keratinocytes. Differentially expressed genes were defined as having a |Log$_2$Fold Change| > 1 and an FDR P-value ≤ 0.05. (D) Venn diagram showing DEGs induced by IFN-λ and IFN-β in WT or knockout keratinocytes. (E) Table of IFN-λ-specific DEGs, their Log$_2$ fold change, and FDR P-value for IFN-λ- and IFN-β-treated WT keratinocytes. (F) Volcano plot showing DEGs after IFN-λ treatment compared to IFN-β treatment in WT and receptor knockout keratinocytes.

(Fig. 6B). The increase in neutrophil frequency in *Ifnlr1*$^{-/-}$ mice corresponded to the kinetics of skin lesion formation, as overall neutrophil frequency was low at 4 dpi, with no significant difference between wild-type and *Ifnlr1*$^{-/-}$ mice, and the increased neutrophil frequency in *Ifnlr1*$^{-/-}$ compared to wild-type mice was first evident during peak disease at 6 dpi and maintained through 8 dpi (Fig. 6B).

To better define the spatial organization of IFN-λ-mediated control of neutrophil infiltration, we harvested skin lesions and healthy skin at 6 dpi from wild-type and *Ifnlr1*$^{-/-}$ mice and evaluated skin pathology by H&E staining (Fig. 6C) and immunohistochemistry for HSV-1 antigen (Fig. 6D). We found that *Ifnlr1*$^{-/-}$ mice displayed more significant skin damage and overall loss or necrosis of the epidermis in their skin lesions compared
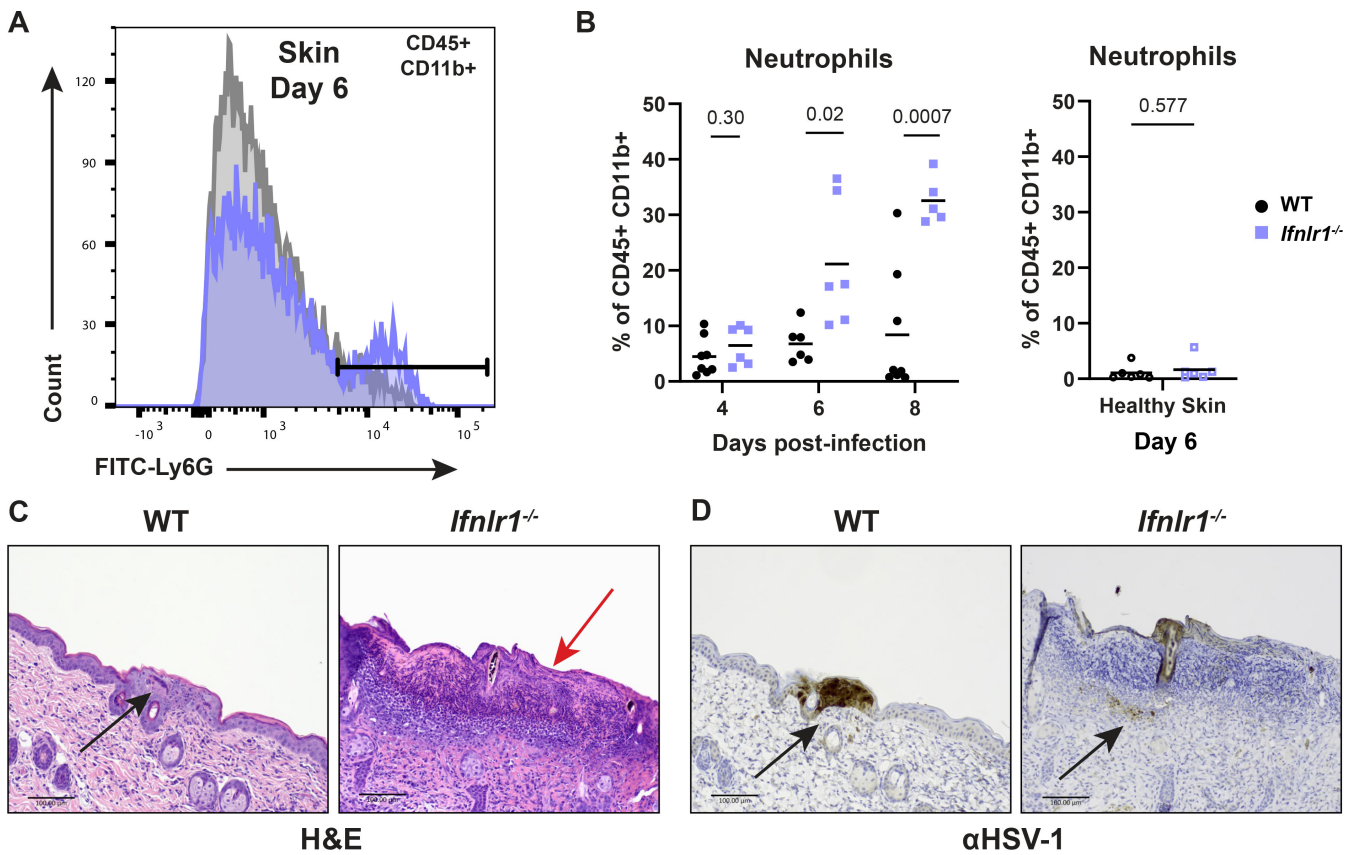

FIG 6 IFN-λ signaling limits neutrophil abundance and severe skin pathology following HSV-1 infection. Eight- to twelve-week-old male and female WT and *Ifnlr1*$^{-/-}$ mice were infected with 10^6 FFU of HSV-1. (A and B) Dermatome lesions and adjacent healthy skin were collected at 4–8 dpi and analyzed by flow cytometry (three independent experiments per time point). (A) Representative histogram of WT and *Ifnlr1*$^{-/-}$ lesions showing Ly6G^{hi} neutrophil gating strategy (CD45+, CD11b+, and Ly6G^{hi}) at 6 dpi. (B) Frequency of neutrophils (Ly6G^{hi} out of CD45+ CD11b+ live cells) for WT and *Ifnlr1*$^{-/-}$ dermatome lesions and adjacent healthy skin. Significant differences in neutrophil frequency were determined using an unpaired t test. P values are reported with $P < 0.05$ considered to be statistically significant. (C and D) Inoculated flank skin was collected at 6 dpi and serial sections of the same skin lesion were processed for histology (six mice per genotype, two independent experiments). (C) H&E staining; the black arrow denotes a neutrophilic pustule, and the red arrow denotes diffuse neutrophilic infiltrate. (D) Anti-HSV-1 immunohistochemistry; viral antigen staining is denoted by black arrows. Scale bars are 100 µm.

to the wild-type mice (Fig. 6C, red arrow). In contrast, wild-type mice had a greater number of intact pustules (Fig. 6C, black arrow) compared to *Ifnlr1*$^{-/-}$ mice, which had a more diffuse spread of neutrophils throughout the dermis and epidermis. Furthermore, wild-type mice also had increased staining intensity for HSV-1 antigen compared to *Ifnlr1*$^{-/-}$ mice, in which most staining was evident within pustules, whereas staining was more diffuse in *Ifnlr1*$^{-/-}$ mice (Fig. 6D). HSV-1 antigen was more present in the dermis for *Ifnlr1*$^{-/-}$ mice (black arrows). However, the epidermis was often missing or necrotic in many areas of intense neutrophilic inflammation in *Ifnlr1*$^{-/-}$ mice, possibly precluding antigen detection in the epidermis. Altogether, these data suggest that a lack of IFN-λ signaling results in greater neutrophil infiltration and more severe HSV-1 skin pathology.

IFN-λ signaling suppresses neutrophil-mediated pathology to limit HSV-1 skin disease

To further define the role of neutrophils in driving HSV-1 skin lesion pathology in the absence of IFN-λ signaling, we depleted neutrophils from wild-type and *Ifnlr1*$^{-/-}$ mice at 0, 2, and 4 dpi using an αLy6G-depleting antibody (or an isotype-control antibody or PBS) and evaluated dermatome skin lesions at 6 dpi (Fig. 7A). To confirm the depletion of circulating neutrophils, we collected splenocytes at 6 dpi (Fig. 7B) and detected neutrophils (Ly6G^{hi}) by flow cytometry. We found that αLy6G antibody efficiently depleted neutrophils compared to isotype-control-treated mice (9.8% vs 0.8% Ly6G^{hi} of CD11b+) (Fig. 7B). We found that neutrophil depletion had no effect on skin lesion area in wild-type mice, consistent with prior studies showing that neutrophils do not mediate HSV-1 skin lesion pathology in wild-type mice (32). However, while we found that *Ifnlr1*$^{-/-}$ mice with an intact neutrophil population (PBS or isotype-control) developed significantly larger lesions than wild-type mice and a greater proportion developed severe lesions, differences in lesion size and disease severity in *Ifnlr1*$^{-/-}$ mice were returned to wild-type levels in neutrophil-depleted mice (Fig. 7C and D). Altogether, these results suggest that IFN-λ protects against severe HSV-1 skin disease by suppressing neutrophil-driven immunopathology.

To determine the mechanism by which IFN-λ suppresses neutrophil-mediated pathology during HSV-1 skin infection, we investigated whether IFN-λ signaling impacts neutrophil recruitment and/or effector function. We infected wild-type and *Ifnlr1*$^{-/-}$ mice with HSV-1 and collected skin lesions at 6 dpi for flow cytometry. We measured the neutrophil expression of lymphocyte function-associated antigen 1 (LFA-1, an integrin upregulated upon neutrophil activation and associated with neutrophil recruitment from circulation into inflamed tissues) and CD63 (a lysosomal membrane protein expressed on primary neutrophil granules that are presented on the plasma membrane upon the final stage of neutrophil degranulation) (Fig. 7E through G) (33–35). We found no significant difference in primary granule release (% LFA-1+ CD63+) between wild-type and *Ifnlr1*$^{-/-}$ mice (65.4% vs 73.3%, *P* > 0.05) (Fig. 7F). However, we found that skin lesions from *Ifnlr1*$^{-/-}$ mice had a greater proportion of LFA-1+ CD63- neutrophils than wild-type mice, indicative of a population of neutrophils in the skin that are activated and accumulating but have not yet fully degranulated (15.2% vs 7.3%, *P* < 0.05; Fig. 7G). Therefore, our data support a model in which IFN-λ signaling suppresses the accumulation, but not effector functions, of neutrophils in HSV-1 skin lesions, protecting against the development of severe skin pathology.

Neutrophils are known to respond to IFN-λ in the context of other infection and inflammation models in mice (16, 36, 37), so we next asked whether the protective effects of IFN-λ against neutrophil-mediated pathology in the skin required IFN-λ signaling directly in neutrophils. We infected conditional knockout mice lacking IFN-λ signaling in myeloid cells (*LysM*-Cre-*Ifnlr1*$^{-/-}$) or neutrophils (*Mrp8*-Cre-*Ifnlr1*$^{-/-}$) with HSV-1 and evaluated skin lesions and disease severity at 6 dpi, compared to wild-type and *Ifnlr1*$^{-/-}$ mice (Fig. 8A through C). We found that mice that lack IFN-λ signaling exclusively in all myeloid cells or specifically in neutrophils developed skin lesions similar in size to *Ifnlr1*$^{-/-}$ mice (mean area 21.5, 19.4, and 25.0 mm^2, *P* > 0.05) (Fig. 8B) and with a
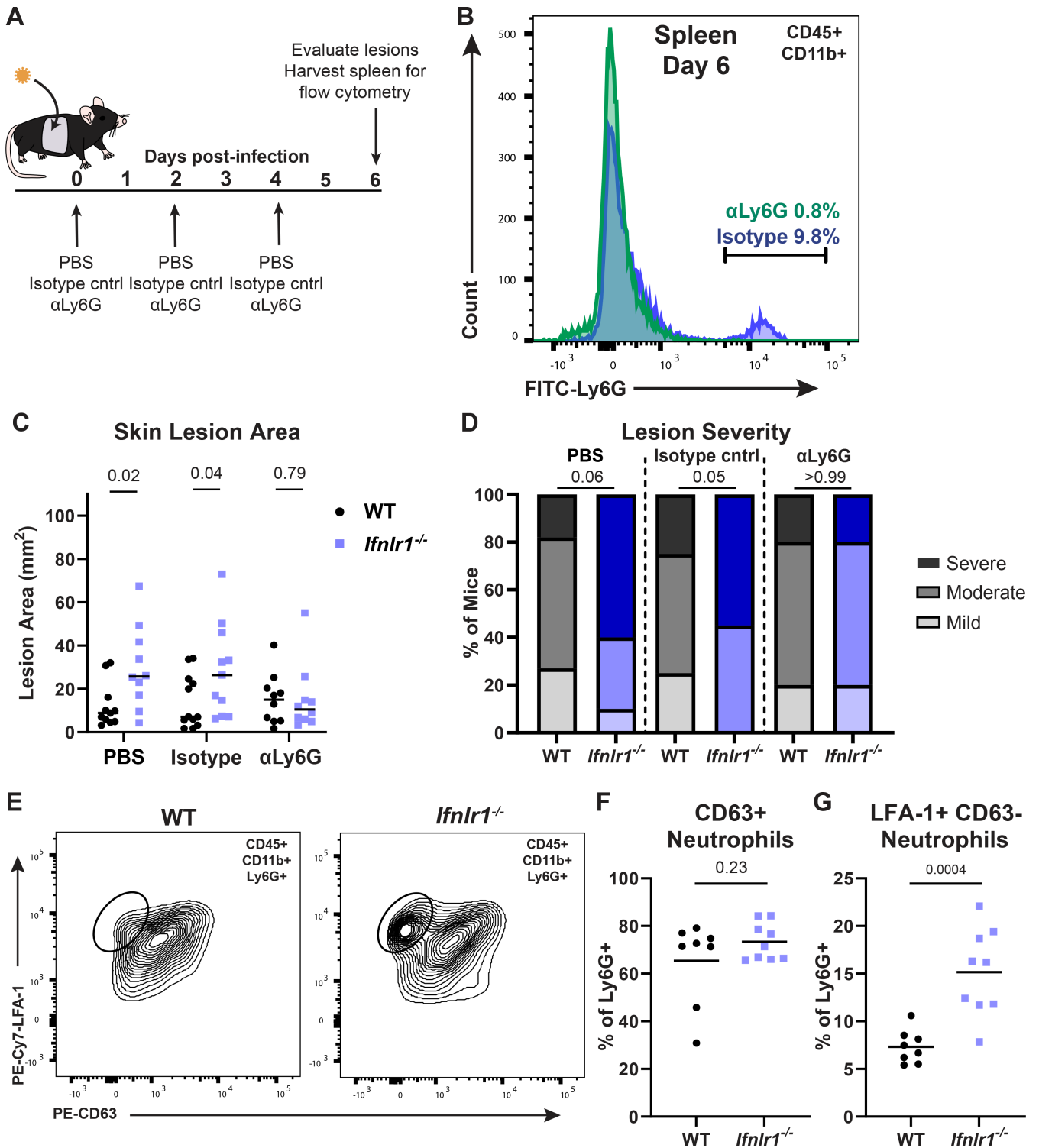
FIG 7 IFN-λ signaling suppresses neutrophil-mediated pathology to limit HSV-1 skin disease. (A) Experimental design for neutrophil depletions. (B–D) WT and *Ifnlr1*⁻/⁻ mice were infected with 10^6 FFU of HSV-1. At 0, 2, and 4 dpi, mice were injected intraperitoneally with PBS, 250 µg of isotype control (IgG2a), or 250 µg of αLy6G (Clone 1A8). (B) Spleens were harvested at 6 dpi and analyzed by flow cytometry to confirm neutrophil depletion. (C) Skin lesions were photographed at 6 dpi, and lesion areas were measured using ImageJ. (D) Skin lesion severity was categorized based on the 6 dpi lesion area. (E–G) WT and *Ifnlr1*⁻/⁻ mice were infected with 10^6 FFU of HSV-1, and at 6 dpi, skin lesions were photographed and analyzed by flow cytometry. (E) Representative plots and gating strategy for (Continued on next page)

FIG 7 (Continued)

neutrophil phenotyping markers LFA-1 and CD63 (percentage of CD45+ CD11b+ Ly6G+). (F) Frequency of CD63+ neutrophils. (G) Frequency of LFA-1+ CD63− neutrophils. Differences in lesion area and viral load were compared by the Mann-Whitney U test, and differences in categorical skin disease were compared by the Cochran-Armitage test. Neutrophil frequencies were compared by unpaired t test. P values are reported with $P < 0.05$ considered to be statistically significant. Data are combined from two to three independent experiments.

similar proportion developing severe lesions (45%, 27%, and 58%, $P > 0.05$) (Fig. 8C). Altogether, these data support a model where IFN-λ signals through keratinocytes and myeloid cells, including neutrophils, to suppress neutrophil accumulation in the skin during HSV-1 infection to control severe HSV-1 skin disease.
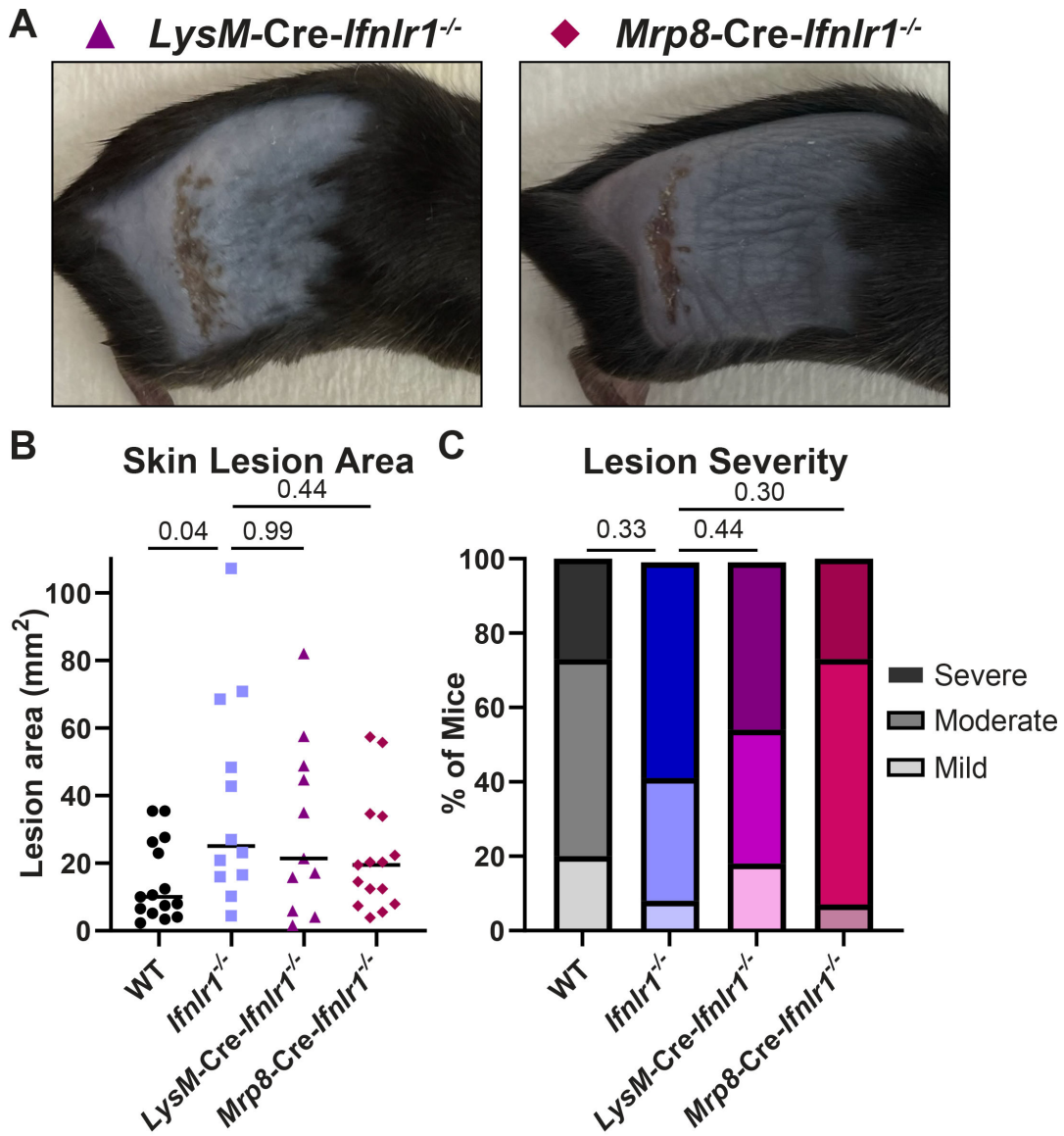

FIG 8 IFN-λ signaling in neutrophils contributes to protection from severe HSV-1 skin disease. Eight- to twelve-week-old male and female WT, *Ifnlr1*^{−/−}, *LysM*-Cre-*Ifnlr1*^{−/−}, and *Mrp8*-Cre-*Ifnlr1*^{−/−} mice were infected with 10^6 FFU of HSV-1. (A) Dermatome skin lesions were photographed at 6 dpi. (B) Skin lesion areas were measured from photographs at 6 dpi using ImageJ. (C) Skin lesion severity was categorized based on the 6 dpi lesion area. Differences in lesion area and viral load were compared by the Mann-Whitney U test. Differences in categorical skin disease were compared by the Cochran-Armitage test. P values are reported with $P < 0.05$ considered to be statistically significant. Data are combined from three to four independent experiments per genotype.

IFN-λ signaling in keratinocytes regulates CXCL9 production to restrict neutrophil infiltration and HSV-1 skin pathology

Having established controlling neutrophil accumulation as a key mechanism of IFN-λ-mediated protection against HSV-1 skin disease, we next sought to determine whether the chemokine CXCL9, identified as a differentially expressed gene in IFN-λ-treated primary keratinocytes (Fig. 5F), mediated neutrophil recruitment in the absence of IFN-λ signaling. Although classically a lymphocyte chemoattractant, neutrophils also are reported to express CXCR3, the receptor for CXCL9, in inflammatory contexts (29, 30, 38–40). Furthermore, Forero et al. (41) previously reported that IFN-λ failed to induce the expression of *Cxcl9* and other chemokines downstream of a lack of IRF1 induction. Therefore, we next asked whether IFN-λ acts through keratinocytes via CXCL9 to limit neutrophil infiltration and severe HSV-1 skin disease. First, we measured the concentration of CXCL9 in dermatome lesions and adjacent healthy skin of wild-type and *Ifnlr1*$^{-/-}$ mice at 6 dpi (Fig. 9A). We found that *Ifnlr1*$^{-/-}$ mice had significantly higher CXCL9 concentrations in their skin lesions compared to wild-type mice (mean 3,191 pg/g vs 1,634 pg/g, $P < 0.05$). The suppressive effect of IFN-λ on CXCL9 was specific to lesion skin because in adjacent healthy skin, CXCL9 concentrations were low and there was no significant difference between wild-type and *Ifnlr1*$^{-/-}$ mice.

Next, we asked whether CXCL9 contributed to neutrophil recruitment and skin pathology and whether this occurred downstream of IFN-λ signaling in keratinocytes. We depleted CXCL9 by injecting wild-type and *K14*-Cre-*Ifnlr1*$^{-/-}$ mice with CXCL9 neutralizing antibody or PBS intraperitoneally at 0, 2, and 4 dpi and assessed lesion area, disease severity, and skin neutrophil populations by flow cytometry (Fig. 9B through D). We did not observe any effect of αCXCL9 treatment on lesion area, disease severity, or neutrophil skin infiltration in wild-type mice. Consistent with prior experiments (Fig. 4), we found that PBS-treated *K14*-Cre-*Ifnlr1*$^{-/-}$ mice had larger lesions and more severe disease than wild-type mice (median lesion area 13.0 vs 6.7 mm^2, $P < 0.05$). We also found that *K14*-Cre-*Ifnlr1*$^{-/-}$ mice had a significantly greater frequency of skin-infiltrating neutrophils compared to wild-type mice (mean neutrophil frequency 31.3% vs 16.9%, $P < 0.05$) (Fig. 9D), although not in absolute number (Fig. S4D). Strikingly, neutralizing CXCL9 ablated these differences, with *K14*-Cre-*Ifnlr1*$^{-/-}$ mice exhibiting similar lesion areas, disease severity, and neutrophil frequency compared to wild-type mice after αCXCL9 treatment (Fig. 9B through D). Altogether, these data suggest that IFN-λ regulates CXCL9 production in keratinocytes, which restricts neutrophil skin infiltration and severe HSV-1 skin disease.

Overall, we report a new protective role for IFN-λ against HSV-1 skin infection. We found that IFN-λ signaling in both keratinocytes and neutrophils is necessary to mediate protection from severe HSV-1 skin disease. We uncovered a mechanism wherein IFN-λ signaling in keratinocytes suppresses CXCL9 production to control neutrophil-mediated pathology by limiting neutrophil recruitment and retention in the skin. This is the first report of a protective role for IFN-λ signaling in the skin against an infection and suggests future opportunities for therapeutic uses of IFN-λ against HSV-1 and other skin pathogens.

DISCUSSION

IFN-λ elicits antiviral immunity and maintains barrier integrity at epithelial surfaces, controlling infections locally without the inflammatory immune pathology triggered by the more potent systemic IFN-αβ response (5). Although IFN-λ induces an antiviral transcriptional program most potently in epithelial cells, IFN-λ signaling in leukocytes, such as neutrophils and dendritic cells, is key to the ability of IFN-λ to induce a protective response without damaging inflammation (26, 36, 37, 42). Despite the well-established role for IFN-λ in antiviral immunity at anatomic barriers (5), including the respiratory and gastrointestinal tracts (13, 43–45), the blood-brain barrier (46, 47), and the maternal-fetal interface (22, 28), the effects of IFN-λ in the skin have not been extensively investigated. To investigate the role of IFN-λ signaling in the skin, we used HSV-1, an important human
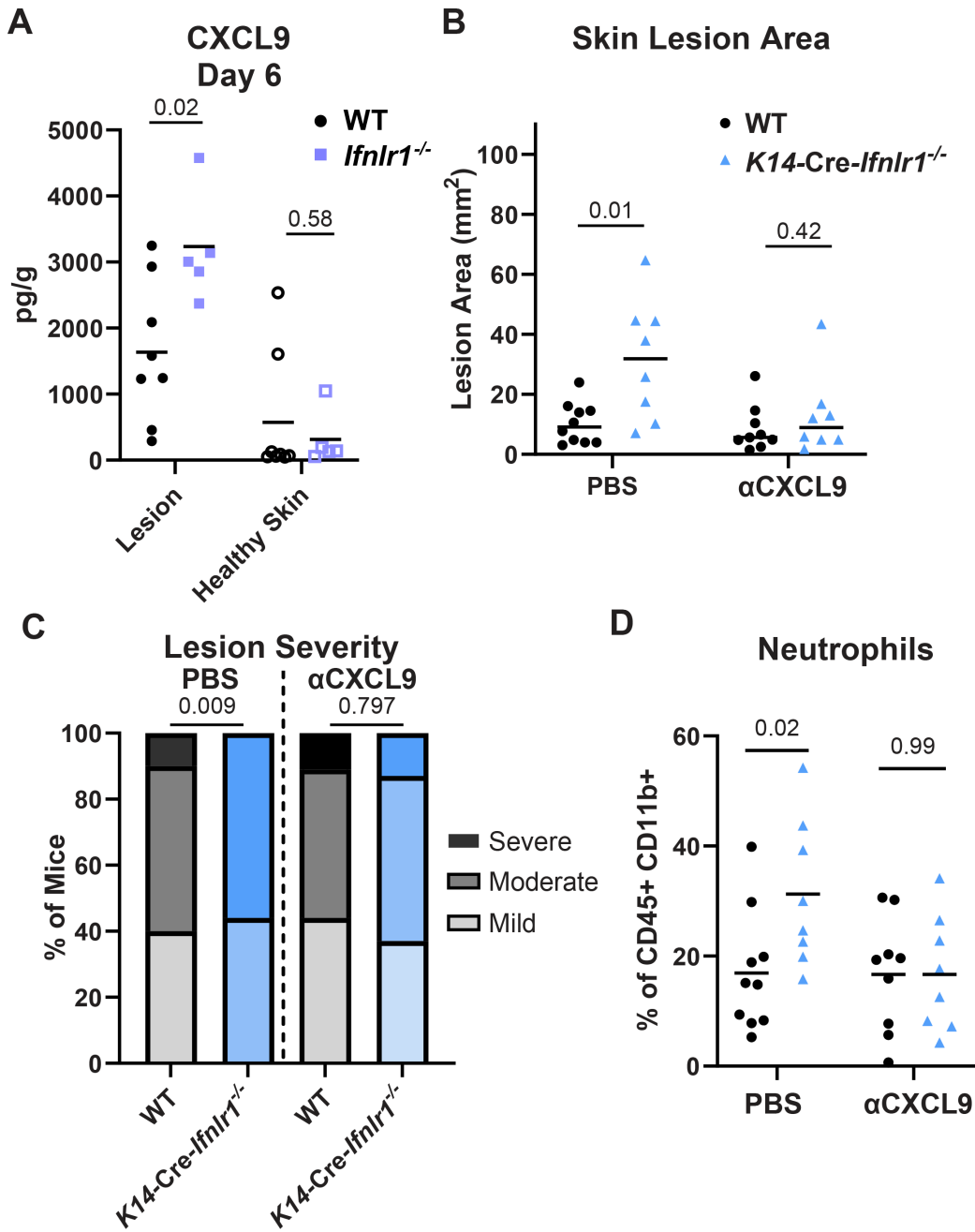
FIG 9 IFN-λ signaling in keratinocytes restricts CXCL9 production to limit neutrophil recruitment and HSV-1 skin disease. Eight- to twelve-week-old male and female mice were infected with 10^6 FFU of HSV-1 and skin lesions were analyzed at 6 dpi. (A) CXCL9 was measured by ELISA in homogenates of lesion skin or adjacent healthy skin from WT and *Ifnlr1*$^{-/-}$ mice. (B–D) WT and *K14*-Cre-*Ifnlr1*$^{-/-}$ mice were infected with HSV-1 and injected intraperitoneally with anti-CXCL9 or PBS at 0, 2, and 4 dpi. Skin lesion areas were measured from photographs at 6 dpi using ImageJ (B), and lesion severity was categorized (C). (D) Neutrophil frequency in skin lesions was measured by flow cytometry at 6 dpi. Differences in lesion area and viral load were compared by the Mann-Whitney *U* test. Differences in categorical skin disease were compared by the Cochran-Armitage test. Differences in CXCL9 concentration and neutrophil frequency were compared by unpaired *t* test. *P* values are reported with *P* < 0.05 considered to be statistically significant. Data are combined from two to three independent experiments.

pathogen that targets epithelial surfaces, including the skin, and has a well-established mouse model for skin infection (9–11). We found that mice lacking IFN-λ signaling (*Ifnlr1*$^{-/-}$, *Ifnl2/3*$^{-/-}$, or *Ifnar1*$^{-/-}$ *Ifnlr1*$^{-/-}$) developed larger HSV-1 skin lesions compared to

their IFN-λ sufficient counterparts. However, lesion size was uncoupled from skin viral loads, suggesting a role for IFN-λ in suppressing inflammatory immune pathology during HSV-1 skin infection. Using conditional knockout mice, we found that IFN-λ signaling in both keratinocytes and leukocytes was necessary for protection from severe skin disease. We further showed that neutrophils are required for the enhanced skin pathology observed in *Ifnlr1*$^{-/-}$ mice and that IFN-λ signaling in neutrophils contributes to the protective effect of IFN-λ against HSV-1 skin disease. Altogether, our results support a model where IFN-λ exerts an immunomodulatory role during HSV-1 skin infection, suppressing neutrophil-mediated pathology.

IFN-λ suppresses neutrophil recruitment and pathology in colitis and rheumatoid arthritis models (16, 36), as well as during influenza virus infection (26). Our results add to a growing number of systems that demonstrate a role for neutrophils as a key IFN-λ responsive cell type in mice and broaden the range of mechanisms by which IFN-λ impacts neutrophil function, although there is still debate regarding the extent to which human neutrophils respond to IFN-λ (36, 37, 48, 49). Neutrophils are recruited to the skin during HSV-1 skin infection but are not important for mediating skin pathology in wild-type mice (32, 50). Our studies revealed a pathogenic role for neutrophils during HSV-1 skin infection but only in the absence of IFN-λ signaling, identifying a key role for IFN-λ in suppressing the pathogenic activity of neutrophils that are recruited into the skin during HSV-1 infection.

While our studies first focused on the protective effects of IFN-λ signaling in leukocytes, specifically neutrophils, we found that IFN-λ signaling in keratinocytes was also required to restrict HSV-1 skin disease. To investigate the mechanism by which IFN-λ signaling in keratinocytes modulates skin immunity to control HSV-1 skin disease, we performed bulk RNA-seq analysis in primary mouse keratinocytes, as well as in a human epithelial cell line (A549). Our data from A549 cells support the standard paradigm that the transcriptional response induced by IFN-λ is less potent than the IFN-β response. However, in primary keratinocytes, we found that many ISGs were induced equivalently by IFN-λ and IFN-β. These observations are consistent with other transcriptional profiling experiments in primary cells (25–28), suggesting that experiments in cell lines may underestimate the potency of the IFN-λ response. A notable difference between the IFN-λ and IFN-β responses in keratinocytes was the chemokine CXCL9, which was only weakly induced by IFN-λ compared to IFN-β, consistent with prior work showing that IFN-λ failed to induce the expression of CXCL9 and other chemokines, downstream of a lack of STAT1 homodimer formation and IRF1 induction (41). Although we found that the IFN-β response was not impacted by the lack of IFN-λ signaling, the IFN-λ response was diminished in both keratinocytes and A549 cells lacking IFN-α/β signaling, suggesting a possible role for cross-talk between the IFN-λ and IFN-α/β responses.

While we found greater accumulation of neutrophils in skin lesions from *Ifnlr1*$^{-/-}$ mice compared to wild-type mice and showed that neutrophils were necessary for the severe skin pathology observed in *Ifnlr1*$^{-/-}$ mice, the mechanism by which IFN-λ modulates neutrophil function to protect against HSV-1 skin disease remains unclear. We found no difference in CD63 expression in neutrophils from *Ifnlr1*$^{-/-}$ mice compared to wild-type mice, suggesting that IFN-λ does not act to inhibit degranulation in this system. We did find that *Ifnlr1*$^{-/-}$ mice exhibited increased expression of the integrin LFA-1, which promotes tissue recruitment and retention of neutrophils, consistent with a model where IFN-λ signaling reduces neutrophil retention in HSV-1 skin lesions. Accordingly, *Cxcl9* was among the genes with reduced induction by IFN-λ compared to IFN-β in primary keratinocytes, CXCL9 levels in skin lesions were higher in the absence of IFN-λ signaling, and depleting CXCL9 ablated the enhanced neutrophil infiltration and large skin lesion phenotypes of *K14*-Cre-*Ifnlr1*$^{-/-}$ mice. Altogether, these data support a model where in the absence of IFN-λ signaling, keratinocytes overproduce CXCL9, stimulating excessive neutrophil infiltration and retention into HSV-1 infected skin, exacerbating skin disease severity.

In addition to HSV-1, we also found a protective role for IFN-λ in HSV-2 skin infection. Like HSV-1, HSV-2 produced larger skin lesions in the absence of IFN-λ signaling, although the average severity of HSV-2 lesions was greater than HSV-1 and the kinetics of the infection were slower. The fact that we observed a similar role for IFN-λ for both HSV-1 and HSV-2 supports a general role for IFN-λ in controlling viral skin infections; future studies will investigate the protective effects of IFN-λ against other viral pathogens that target the skin, including poxviruses, papillomaviruses, and arboviruses, as well as bacterial, fungal, and protozoan skin pathogens. We also evaluated whether IFN-λ protected against HSV vaginal infection since the vaginal epithelium is a plausible site for IFN-λ activity and IFN-λ has been reported to protect against vaginal HSV-2 and Zika virus infections (25, 51). HSV-1 vaginal infection typically does not produce overt disease in mice, whereas HSV-2 produces disease signs that can be evaluated in addition to measuring viral loads. Prior work with HSV-2 vaginal infection in wild-type mice showed that neutrophil recruitment to the vagina worsened disease severity (52), further supporting the premise for a protective role for IFN-λ at this epithelial barrier. However, we found no difference in overt vaginal disease in *Ifnlr1*$^{-/-}$ mice compared to wild-type mice infected with HSV-2. These results are consistent with our previous observations with Zika virus, where we found no difference in vaginal wash viral loads from *Ifnlr1*$^{-/-}$ mice compared to wild-type mice (53). Additionally, our data are consistent with other reports for Zika virus and HSV-2 vaginal infections, as these experiments only found protective effects for IFN-λ signaling when pretreating mice intravaginally with recombinant IFN-λ or Toll-like receptor 3 (TLR-3) or TLR-9 agonists (25, 51), as opposed to evaluating phenotypes in *Ifnlr1*$^{-/-}$ mice. Overall, these observations suggest any protective effect of IFN-λ in the vagina may be context-dependent and likely does not serve to restrict viral replication. The difference in phenotypes for IFN-λ signaling against HSV-2 infection in the skin and the vagina also underscores possible differences in mechanisms of immunity at these different epithelial barriers.

Although our work has focused on IFN-λ-mediated protection from HSV-1 in the context of healthy skin, it will be interesting to evaluate these effects in the context of dermatological conditions such as atopic dermatitis (also called eczema). Patients with atopic dermatitis are susceptible to severe HSV-1 skin infections (eczema herpeticum) (54). Notably, atopic dermatitis skin lesions exhibit diminished IFN-λ production compared to healthy skin from the same patients (55), and injection of recombinant IFN-λ reduced the severity of eczema herpeticum in mice (56). Atopic dermatitis patients also are susceptible to severe infections by poxviruses, posing a hazard to individuals who require smallpox vaccination (due to the risk of exposure to or laboratory work with variola virus, vaccinia virus, or other orthopoxviruses) (57, 58). We expect that the mechanisms by which IFN-λ restricts HSV-1 skin disease will be relevant to other skin infections, particularly where pathogen-triggered immune pathology produces skin lesions, such as vaccinia virus and *Leishmania* (59, 60).

We found that *Ifnlr1*$^{-/-}$ mice developed larger HSV-1 skin lesions compared to wild-type mice, even though there was no difference in viral loads in the skin, supporting an immunomodulatory, rather than antiviral, role for IFN-λ in the skin. However, in this system, IFN-λ is induced in the skin in response to HSV-1 infection, meaning that the virus has a head start and can employ its arsenal of strategies to antagonize the host IFN response. When we instead pre-treated mice with topical IFN-λ prior to infection, we found lower viral loads in IFN-λ-treated mice compared to PBS-treated mice, indicating that IFN-λ can have an antiviral effect against HSV-1 in the skin. IFN-λ has demonstrated therapeutic utility against a variety of viral infections in human studies, including hepatitis C virus, hepatitis B virus, and SARS-CoV-2, as it is thought to confer protective antiviral activity without the damaging immune pathology induced by IFN-α/β treatment (5, 18). The skin is an especially attractive site to leverage the protective effects of IFN-λ, due to its easy accessibility for topical administration. Encouragingly, topical IFN-λ treatment restricted HSV-1 corneal infection in mice (61). Future studies will

investigate the potential for topical IFN-λ treatment as a therapy for HSV and other skin infections.

Altogether, our data provide the first evidence of a skin-specific role for IFN-λ in controlling a viral infection. We detail a mechanism by which IFN-λ signals through both keratinocytes and leukocytes to limit severe HSV-1 skin disease. We found that IFN-λ signaling suppresses neutrophil recruitment to the skin, in part by suppressing CXCL9, and the excess recruitment of neutrophils to the skin in the absence of IFN-λ signaling is the driver of pathology. This keratinocyte-neutrophil axis via CXCL9 provides new insights into the immunomodulatory effects of IFN-λ at barrier sites, including the skin.

MATERIALS AND METHODS

Viruses and cells

Virus stocks were grown in Vero (African green monkey kidney epithelial) cells. Vero and A549 (ATCC# CCL-185) cells were maintained in Dulbecco's modified Eagle medium (DMEM) containing 5% heat-inactivated fetal bovine serum (FBS) and L-glutamine at 37°C with 5% CO_2. Virus stocks were grown in DMEM containing 2% FBS, L-glutamine, and HEPES at 37°C with 5% CO_2. HSV-1 strain NS was obtained from Dr. Harvey Friedman (University of Pennsylvania) [62]. HSV-2 strain 333 was obtained from Dr. Steven Bachenheimer (UNC). Virus stock titers were determined by focus-forming assay on Vero cells. Viral foci were detected using 1:10,000 dilution of αHSV rabbit antibody (Dako) and 1:50,000 dilution of goat αrabbit HRP-conjugated antibody and TrueBlue peroxidase substrate (KPL). Antibody incubations were performed for at least 1 hour at room temperature. Foci were counted on a CTL Immunospot analyzer.

Mice

Experiments used 8–12-week-old male and female mice on a C57BL/6 background. Wild-type mice used in Fig. 3 and Fig. S1 originally were purchased from Jackson Labs and then bred in-house. *Ifnlr1*$^{-/-}$ mice were generated by two breeding schemes. For *Ifnlr1*$^{-/-}$ mice in Fig. 1 and Fig 5-7, mice were generated by crossing *Ifnlr1*$^{f/f}$ mice with mice expressing Cre recombinase under the control of an actin promoter. These mice were bred as Cre hemizygotes to generate mixed litters in which 50% of mice retained IFN-λ signaling and 50% lacked IFN-λ signaling. For *Ifnlr1*$^{-/-}$ mice in Fig. 4 and 8, mice were generated by crossing *Ifnlr1*$^{f/f}$ mice with mice expressing Cre recombinase under the control of a CMV promoter. After generation, mice were bred as knockout by knockout and experimental *Ifnlr1*$^{-/-}$ mice were genotyped periodically to verify *Ifnlr1* knockout status. *K14*-Cre-*Ifnlr1*$^{-/-}$, *Vav*-Cre-*Ifnlr1*$^{-/-}$, *LysM*-Cre-*Ifnlr1*$^{-/-}$, and *Mrp8*-Cre-*Ifnlr1*$^{-/-}$ mice were generated by crossing *Ifnlr1*$^{f/f}$ mice with mice expressing Cre recombinase under the control of a *Vav* promoter (Jackson Labs #8610), a *Krt14* promoter (obtained from Dr. Scott Williams, UNC), a LysM promoter (Jackson Labs #4781, obtained from Dr. Jenny Ting, UNC), or a *Mrp8* promoter (Jackson Labs #21614), respectively. Mice were bred as Cre hemizygotes to generate mixed litters in which 50% of mice retained IFN-λ signaling and 50% lacked IFN-λ signaling in specific cell types. After data analysis, experimental mice were genotyped by PCR on tails for both Cre and *Ifnlr1*. *Ifnar1*$^{-/-}$ mice were obtained from Dr. Jason Whitmire (UNC) and then bred in-house. *Ifnar1*$^{-/-}$ *Ifnlr1*$^{-/-}$ DKO mice were generated by crossing *CMV*-Cre *Ifnlr1*$^{-/-}$ and *Ifnar1*$^{-/-}$ mice and bred in-house. *Ifnl2/3*$^{-/-}$ mice were obtained from Dr. Megan Baldridge (Washington University in St. Louis) and then bred in-house.

Ifnk$^{-/-}$ mice were generated in the laboratory of Dr. Michael Diamond (Washington University in St. Louis). Embryonic stem (ES) cells (C57BL/6 background) were obtained from the knockout mouse project (KOMP). The ES cells contained a LacZ reporter-tagged deletion allele with a neomycin selection cassette [Ifnk$^{tm1(KOMP)Vlcg}$]. Mice derived from these ES cells were crossed to mice expressing Cre recombinase under a CMV promoter to excise the neomycin selection cassette. The resulting *Ifnk*$^{-/-}$ mice were bred at UNC for

use in experiments. Genetic background was confirmed by the miniMUGA genotyping array.

HSV skin infections

One day prior to infection, mice were anesthetized by nose-cone isoflurane and depilated manually by plucking the fur from the right flank. One day later, mice were anesthetized by chamber isoflurane for infections. To perform infections, we abraded the skin of anesthetized, depilated mice with ~10 closely spaced punctures (over ~5 mm^2) using a Quintip skin test allergy needle. Immediately after abrasion, we overlaid 10 µL of viral inoculum (virus + 1% FBS in PBS) and allowed the inoculum to dry while the mice were anesthetized.

PCR genotyping

Ifnlr1, *Cre*, *Ifnl2/3*, and *Ifnk* genotypes were determined by PCR on tail samples (unless otherwise indicated) on DNA extracted using the Quantabio supermix and the following previously described primers:

Ifnlr1 $F_1$5′-AGGGAAGCCAAGGGGATGGC-3′, $R_1$5′-AGTGCCTGCTGAGGACCAGGA-3′, $R_2$5′-GGCTCTGGACCTACGCGCTG-3′;

Cre $F_1$5′-CGTACTGACGGTGGGAGAAT-3′, $R_1$5′-CCCGGCAAAACAGGTAGTTA-3′;

Ifnl2/3 F_{KO}5′-CACACTGTGGACAGGCCAT-3′, R_{KO}5′-ACCAGCCTGAGGTCCCTAGT-3′, F_{WT}5′-TGGAGTCCAGAGCAGCTTTT-3′, R_{WT}5′-TCCACCCAGAAGCAAAGAAC-3′;

Ifnk $F_1$5′-CCTGTGTGTCAGGTTTAC-3′, $R_1$5′-TGCCCAACTCCAGGTAGAC-3′, $R_2$5′-GTCTGTC CTAGCTTCCTCACTG –3′;

K14-Cre $F_1$5′- CACGATACACCTGACTAGCTGGGTG-3′, $R_1$5′- CATCACCCACAGGCTAGCGC CAACT-3′;

Vav-Cre $F_1$5′- AGATGCCAGGACATCAGGAACCTG-3′, $R_1$5′- ATCAGCCACACCAGACACAGA GATC-3′.

Focus-forming assay

Viral loads were measured by focus-forming assay in which tissues were weighed, homogenized using beads and DMEM with 2% FBS and 1% HEPES, and serially diluted in a round bottom 96-well plate. A volume of 100 µL of each dilution was then transferred to monolayers of Vero cells (96-well plate with 2×10^4 cells/well plated 1 day prior) in duplicate and incubated at 37℃ for 1 hour. Thereafter, wells were overlaid with 125 µL of methylcellulose (1% methylcellulose in 1× MEM + 2% FBS, L-Glut, P/S, HEPES) and left to incubate at 37℃ for 20 hours. After 20 hours, the plates were fixed by adding 4% paraformaldehyde (PFA) 100 µL/well for 1 hour at room temperature. After fixing, PFA and overlay were flicked off, and the plates were washed 3× with PBS + 1% Tween using a handheld plate washer. Foci were detected using 1:10,000 dilution of αHSV rabbit antibody (Dako) and 1:50,000 dilution of goat αrabbit HRP-conjugated antibody and TrueBlue peroxidase substrate (KPL). Antibody incubations were performed for at least 1 hour at room temperature. Foci were counted on a CTL Immunospot analyzer.

Viral genome quantification by qPCR

Viral genomes were quantified from pooled DRG samples (L2–L5 from the ipsilateral or contralateral sides) that were homogenized in 500 µL of PBS and beads. DNA was extracted from 200 µL of homogenate using the Qiagen DNeasy Blood & Tissue Kit (#69504). HSV-1 DNA was quantified by TaqMan qPCR on a CFX96 Touch real-time PCR detection system (Bio-Rad) against a standard curve generated by extracting DNA from an HSV-1 viral stock. HSV-1 genomes were detected using the following primers targeting the U_L23 gene: F primer 5′-TTGTCTCCTTCCGTGTTTCAGTT-3′, R primer 5′-GGC TCCATACCGACGATCTG-3′, and probe 5′-FAM-CCATCTCCCGGGCAAACGTGC-MGB-NFQ-3′ (63).

Lesion area quantification and categorization

To measure HSV lesion areas, mice were anesthetized and photographed using an iPhone camera next to a ruler and an identifying card. Thereafter, images were analyzed using ImageJ, in which pixels were converted to millimeters using the reference ruler, and then lesions were outlined using the freehand tool, and the calculated area within the freehand designations was reported. Lesions analyzed at 6 dpi were categorized using the following system: <5 mm^2 = mild, 5–23 mm^2 = moderate, and >23 mm^2 = severe.

HSV-2 vaginal infections and disease categorization

To infect mice with HSV-2 vaginally, experimental mice were treated 5 days prior with 2 mg DepoProvera (UNC Pharmacy) via subcutaneous inoculation. On the day of infection, mice were inoculated with 10^3 FFU/10 µL of HSV-2 strain 333 intravaginally. Mice were monitored for disease signs starting at 4 dpi and categorized using the following scoring system (52): 0: no inflammation, 1: mild redness and swelling, 2: visible ulceration and fur loss, 3: severe ulceration and signs of sickness, 4: hindlimb paralysis, and 5: moribund/dead.

Bone marrow chimeras

Bone marrow chimera mice were generated by lethally irradiating wild-type and *Ifnl2/3*$^{-/-}$ mice (2 × 600 CGy) and injecting 10^7 bone marrow cells from complementary and reciprocal donors. After irradiation, mice were given sulfamethoxazole (6 mg/mL) in their drinking water for the duration of their life. Mice were infected with HSV-1 and photographed and harvested at 6 dpi. Efficient bone marrow transfer was validated at the end of the experiment by PCR genotyping tail, ear skin, and whole blood from each mouse for *Ifnl2/3*.

Flow cytometry

For analysis by flow cytometry, tissues were harvested into cold DMEM + 10% FBS and processed using established methods for digestion of whole mouse back skin (64). In brief, samples were cut into thirds and incubated overnight at 4°C in 5 mg/mL Dispase II (Sigma) in Hanks Buffered Salt Solution. Afterward, samples were washed 1× with cold PBS, and the epidermis and dermis were mechanically separated for separate enzymatic digestions. The epidermis was digested in 1 mL of 0.05% trypsin (Fisher) for 30 min at 37°C. Separately, the dermis was digested in 3 mL of dermal dissociation solution [1 mg/mL Collagenase P (Sigma), 100 µg/mL DNase I (Fisher) for 1 hour at 37°C]. After incubation, matched epidermal and dermal digestions were combined and passed through a 70 µm cell strainer and resuspended in DMEM + 10% FBS. Suspensions were then centrifuged at 400 × *g* for 5 min at 4°C and resuspended in PBS + 1% FBS (staining buffer) and stained with fluorescent antibodies.

Fc Block and all fluorescent antibodies were sourced from BioLegend and titrated prior to use. Samples were treated with Fc Block for 10 min at 4°C prior to staining. Afterward, samples were washed 3× in staining buffer and then stained for cell surface antigens for 20 min at 4°C. Cells were then washed 3×, fixed with 2% paraformaldehyde solution, and analyzed on an LSRII (BD). Data were analyzed with FlowJo software (v10.8). The following fluorescent antibodies (and specific clones) were used: αCD3 (145–2C11), αEPCAM (G8.8), αCD8a (54–6.7), αCD4 (CK1.5), αCD45 (30-F11), αNK1.1 (PK136), αLy6G (IA8), αCD11c (N418), Fc Block αCD16/32 (93), αCD11b (M1/70), αCD19 (6D5), αLy6C (HK1.4) αCD63 (NVG-2), αLFA-1 (H155-78), and Zombie UV Fixable Dye. Gating strategies for neutrophils are shown in Fig. S3. All gating strategies for all cell types and neutrophil phenotyping markers were based on published immunophenotyping methods (33, 64, 65).

Histopathology

Samples were prepared for histology by collecting the entire depilated region of the right flank (lesional and healthy skin), flattening the skin on cardstock, and submerging in 10% neutral buffered formalin for 48 hours at 4°C. After fixation, skins were washed and resuspended in 70% ethanol and stored at 4°C until submission to the UNC Pathology Services Core Facility. To prepare fixed skin for submission, two cuts of skin were taken: (i) a horizontal section through the flank to capture lesions and healthy skin, and (ii) a vertical cut to capture the diseased dermatome region of skin. Thereafter, samples were stored in 70% ethanol and processed by the core, stained for H&E and HSV-1 (1:1,000, Dako), and analyzed by a veterinary pathologist (Dr. Hannah Atkins), who selected representative images and identified regions of interest.

Neutrophil and CXCL9 depletions

To deplete neutrophils, mice were injected intraperitoneally at 0, 2, and 4 dpi with 250 µg in 200 µL of αLy6G antibody (Clone 1A8 IgG2a, BioXCell) or with isotype control antibody (BioXCell) or PBS. Systemic depletion of neutrophils was validated at the end of the experiment in each cohort of mice using the gating strategy outlined in Fig. S3B on splenocytes. To neutralize CXCL9, mice were injected intraperitoneally at 0, 2, and 4 dpi with 300 µg in 200 µL of αCXCL9 antibody (Clone MIG-2F5.5 IgG, BioXCell).

CXCL9 ELISA

To measure the concentration of CXCL9 in the skin, lesional and healthy skin were collected from wild-type and $Ifnlr1^{-/-}$ mice at 6 dpi. Samples were weighed and then homogenized using beads and resuspended in 1 mL of DMEM. CXCL9 was measured from homogenized skin supernatants using the MIG/CXCL9 Mouse ELISA Kit (Thermo-Fisher, #EMCXCL9) using optical density read at 450 nm and fit against the standard curve according to manufacturer protocol.

IFN-λ topical pre-treatment

To prophylactically treat mice with IFN-λ, mice were depilated by plucking 2 days prior to infection. The next day, 5 µg of recombinant murine IFN-λ3 (PBL #12820) in 10 µL of PBS (or PBS alone) was applied topically to a 5 mm^2 region of skin and allowed to air dry. The treated area of skin was circled with a Sharpie, and 24 hours, later mice were infected with HSV-1 at the treated site.

Generating IFN receptor knockout A549 cell lines

IFN receptor knockout cell lines were generated in an A549 background using CRISPR/Cas9 gene editing. A single guide RNA targeting exon 2 of IFNAR1 (5′-CACCGTAGATGACAACTTTATCCTG-3′), exon 3 of IFNLR1 (5′-CACCGACAAGTTCAAGGGACGCGTG-3′), and a non-targeting control (5′-CACCGGTATAATACACCGCGCTAC-3′) were cloned into the lentiCRISPRv2 vector (Addgene). The gRNA construct was then co-transfected with two packaging plasmids (pMD2.G and pSPAX2, Addgene) into HEK293T cells to produce lentiviruses. A549 cells were transduced and selected using 2.5 µg/mL puromycin for 2 weeks. Surviving cells were then single-cell sorted into 96-well plates using a FACS ARIA II flow cytometer. Single clones of knockout monoclonal cultures were confirmed via Sanger sequencing and used for subsequent experiments.

Primary mouse keratinocyte isolation

Keratinocytes were isolated from adult male and female mice of indicated genotypes using published protocols (66). In brief, mice were euthanized and whole tails were harvested into cold PBS. Tail skin was peeled off, cut into thirds, and digested overnight at 4°C in 4 mg/mL of Dispase II (Sigma) while rotating. The epidermis was then mechanically peeled from the dermis and placed basal side down into 0.05% trypsin to shake for

20 min at room temperature. Afterward, 7 mL of DMEM with 10% FBS was added, and the epidermis was rubbed basal side down into the bottom of a petri dish to release basal keratinocytes. Cell suspensions were collected, passed through a 70 µm cell strainer, and pelleted at $400 \times g$ for 5 min. Cell pellets were resuspended in DermaLife K Keratinocyte Medium without antibiotics (Lifeline, Cat #LL-007) to 1×10^5 cells/mL and seeded 1 mL/well in 12-well plates. One adult mouse tail generally yields $\sim 1 \times 10^5$ cells. Keratinocytes were grown to confluence, ~3–4 days, with media changes every other day, prior to experimental use.

IFN treatments in cell culture

Primary mouse keratinocytes in 12-well plates were grown to confluence for 3–4 days after isolation. Recombinant murine IFN-β (5 ng/mL; PBL #12401) or IFN-λ3 (5 ng/mL; PBL# 12820) was resuspended in fresh keratinocyte growth media, and 1 mL of IFN suspension or media alone was added to cells. Twenty-four hours later, the supernatant was removed, 350 µL of Buffer RLT (Qiagen) was added to each well, and samples were stored at −80℃ until RNA extraction. A549 cells were treated similarly at confluence in 6-well plates with recombinant human IFN-β (5 ng/mL; PBL #11415) or IFN-λ2 (50 ng/mL; PBL #11720) or media only, resuspended in A549 growth media. Then, 8 hours later, the supernatant was removed, 350 µL of Buffer RLT (Qiagen) was added to each well, and samples were stored at −80℃ until RNA extraction.

RNA extractions and RT-qPCR

RNA from primary keratinocytes and A549 cells was extracted with the Qiagen RNAeasy minikit. Predesigned primer/probe sets (Integrated DNA Technologies) were used to detect murine *Ifit1* (Mm.PT.58.32674307) and *ActB* (Mm.PT.39a.22214843.g) and human *IFIT1* (Hs.PT.56a.20769090.g) and *ACTB* (Hs.PT.39a.22214847). Transcripts were measured by TaqMan one-step RT-qPCR on a CFX96 Touch real-time PCR detection system (Bio-Rad) and were reported as relative differences in threshold cycle (Ct) values between ISG and actin as a housekeeping gene using the $2^{-\Delta\Delta Ct}$ with reference to the average of media-treated, wild-type primary keratinocytes or RenLuc A549s for each sample.

RNA sequencing

RNA extracted from A549 cells and primary keratinocytes with the indicated IFN treatments was prepared for RNA sequencing by the UNC High Throughput Sequencing Facility using the Kapa mRNA-stranded Library Prep Kit. Primary keratinocytes were sequenced using NovaSeq6000S4 XP Paired End 2×100, and A549 cells were sequenced using NovaSeq6000S4 XP Paired End 2×150. Sequences were analyzed using CLC Genomics Workbench version 23.0.4 (Qiagen) with references to *Mus musculus* reference genome sequence and annotation mm10 (Ensembl GRCm39.110) and *Homo sapiens* reference genome sequence and annotation hg38 (Ensembl GRCh38.110) for sequences from primary keratinocytes and A549 cells, respectively, using default settings. Gene lists were then analyzed using principal component analysis and volcano plot tools within the CLC Genomics Workbench. Differentially expressed genes were defined by having a false discovery rate < 0.05 and an absolute value Log_2 Fold Change > 1. Statistics were calculated within the CLC Genomics Workbench, and volcano plots were prepared for visualization using GraphPad Prism 9 and principal component analysis plots using the CLC Genomics Workbench. Raw and processed RNA sequencing data are available under the GEO superseries accession number GSE242171.

Statistics

All statistics (apart from RNAseq data) were calculated using GraphPad Prism 9 or XLSTAT 2022 Plugin. Lesion area, viral loads, and vaginal disease score were analyzed using a Mann-Whitney *U* test and adjusting for multiple comparisons using the Holm-Šídák method when appropriate. Flow cytometry was analyzed using an unpaired *t*-test. HSV-1

skin disease severity was analyzed using the Cochrane-Armitage method and adjusting for multiple comparisons using the Benjamini and Hochberg method when appropriate. Survival curves were analyzed using the Mantel-Cox Log Rank test.

AUTHOR AFFILIATIONS

[1]Department of Microbiology and Immunology, University of North Carolina at Chapel Hill, Chapel Hill, North Carolina, USA

[2]Department of Epidemiology, School of Public Health, University of North Carolina at Chapel Hill, Chapel Hill, North Carolina, USA

[3]Department of Genetics, University of North Carolina at Chapel Hill, Chapel Hill, North Carolina, USA

[4]Department of Pathology and Laboratory Medicine, University of North Carolina at Chapel Hill, Chapel Hill, North Carolina, USA

AUTHOR ORCIDs

Drake T. Philip http://orcid.org/0000-0002-6394-7686
Nigel M. Goins http://orcid.org/0009-0002-7000-8211
Nicholas J. Catanzaro http://orcid.org/0000-0002-0210-8440
Ichiro Misumi http://orcid.org/0000-0003-3892-7605
Jason K. Whitmire http://orcid.org/0000-0003-2578-6073
Hannah M. Atkins http://orcid.org/0000-0001-7689-1477
Helen M. Lazear http://orcid.org/0000-0002-8649-4579

ETHICS APPROVAL

All experiments and husbandry were performed under the approval of the University of North Carolina at Chapel Hill Institutional Animal Care and Use Committee.

ADDITIONAL FILES

The following material is available online.

Supplemental Material

Fig. S1 (mBio02623-23-s0001.tif). Optimizing an HSV-1 skin infection model.
Fig. S2 (mBio02623-23-s0002.tif). Validation of keratinocyte-specific Ifnlr1 conditional knockouts.
Fig. S3 (mBio02623-23-s0003.tif). IFN-λ and IFN-β induced transcriptional responses in A549 cells.
Fig. S4 (mBio02623-23-s0004.tif). Immunophenotyping of skin tissues from WT and Ifnlr1-/- mice.
Fig. S5 (mBio02623-23-s0005.tif). Representative gating strategy to define neutrophil populations.
Table S1 (part 1) (mBio02623-23-s0006.xlsx). RNAseq data from A549 cells (part 1).
Table S1 (part 2) (mBio02623-23-s0007.xlsx). RNAseq data from A549 cells (part 2).
Table S1 (part 3) (mBio02623-23-s0008.xlsx). RNAseq data from A549 cells (part 3).
Table S2 (mBio02623-23-s0009.xlsx). RNAseq data from primary keratinocytes.

REFERENCES

1. Handfield C, Kwock J, MacLeod AS. 2018. Innate antiviral immunity in the skin. Trends Immunol 39:328–340. https://doi.org/10.1016/j.it.2018.02.003

2. Nestle FO, Di Meglio P, Qin J-Z, Nickoloff BJ. 2009. Skin immune sentinels in health and disease. Nat Rev Immunol 9:679–691. https://doi.org/10.1038/nri2622

3. Kobayashi T, Naik S, Nagao K. 2019. Choreographing immunity in the skin epithelial barrier. Immunity 50:552–565. https://doi.org/10.1016/j.immuni.2019.02.023

4. Mesev EV, LeDesma RA, Ploss A. 2019. Decoding type I and III interferon signalling during viral infection. Nat Microbiol 4:914–924. https://doi.org/10.1038/s41564-019-0421-x

5. Lazear HM, Schoggins JW, Diamond MS. 2019. Shared and distinct functions of type I and type III Interferons. Immunity 50:907–923. https://doi.org/10.1016/j.immuni.2019.03.025

6. Dowling JW, Forero A. 2022. Beyond good and evil: molecular mechanisms of type I and III IFN functions. J Immunol 208:247–256. https://doi.org/10.4049/jimmunol.2100707

7. Kollias CM, Huneke RB, Wigdahl B, Jennings SR. 2015. Animal models of herpes simplex virus immunity and pathogenesis. J Neurovirol 21:8–23. https://doi.org/10.1007/s13365-014-0302-2

8. Bradley H, Markowitz LE, Gibson T, McQuillan GM. 2014. Seroprevalence of herpes simplex virus types 1 and 2--United States, 1999-2010. J Infect Dis 209:325–333. https://doi.org/10.1093/infdis/jit458

9. Simmons A, Nash AA. 1984. Zosteriform spread of herpes simplex virus as a model of recrudescence and its use to investigate the role of immune cells in prevention of recurrent disease. J Virol 52:816–821. https://doi.org/10.1128/JVI.52.3.816-821.1984

10. van Lint A, Ayers M, Brooks AG, Coles RM, Heath WR, Carbone FR. 2004. Herpes simplex virus-specific CD8+ T cells can clear established lytic infections from skin and nerves and can partially limit the early spread of virus after cutaneous inoculation. J Immunol 172:392–397. https://doi.org/10.4049/jimmunol.172.1.392

11. Wang P, Gamero AM, Jensen LE. 2019. IL-36 promotes anti-viral immunity by boosting sensitivity to IFN-α/β in IRF1 dependent and independent manners. Nat Commun 10:4700. https://doi.org/10.1038/s41467-019-12318-y

12. Broggi A, Granucci F, Zanoni I. 2020. Type III interferons: balancing tissue tolerance and resistance to pathogen invasion. J Exp Med 217:e20190295. https://doi.org/10.1084/jem.20190295

13. Peterson ST, Kennedy EA, Brigleb PH, Taylor GM, Urbanek K, Bricker TL, Lee S, Shin H, Dermody TS, Boon ACM, Baldridge MT. 2019. Disruption of type III interferon (IFN) genes Ifnl2 and Ifnl3 recapitulates loss of the type III IFN receptor in the mucosal antiviral response. J Virol 93:e01073-19. https://doi.org/10.1128/JVI.01073-19

14. Gharaee-Kermani M, Estadt SN, Tsoi LC, Wolf-Fortune SJ, Liu J, Xing X, Theros J, Reed TJ, Lowe L, Gruszka D, Ward NL, Gudjonsson JE, Kahlenberg JM. 2022. IFN-K is a rheostat for development of psoriasiform inflammation. J Invest Dermatol 142:155–165. https://doi.org/10.1016/j.jid.2021.05.029

15. LaFleur DW, Nardelli B, Tsareva T, Mather D, Feng P, Semenuk M, Taylor K, Buergin M, Chinchilla D, Roshke V, Chen G, Ruben SM, Pitha PM, Coleman TA, Moore PA. 2001. Interferon-kappa, a novel type I interferon expressed in human keratinocytes. J Biol Chem 276:39765–39771. https://doi.org/10.1074/jbc.M102502200

16. Blazek K, Eames HL, Weiss M, Byrne AJ, Perocheau D, Pease JE, Doyle S, McCann F, Williams RO, Udalova IA. 2015. IFN-λ resolves inflammation via suppression of neutrophil infiltration and IL-1β production. J Exp Med 212:845–853. https://doi.org/10.1084/jem.20140995

17. Dinnon KH III, Leist SR, Schäfer A, Edwards CE, Martinez DR, Montgomery SA, West A, Yount BL Jr, Hou YJ, Adams LE, Gully KL, Brown AJ, Huang E,

Bryant MD, Choong IC, Glenn JS, Gralinski LE, Sheahan TP, Baric RS. 2020. A mouse-adapted model of SARS-CoV-2 to test COVID-19 countermeasures. Nature 586:560–566. https://doi.org/10.1038/s41586-020-2708-8

18. Feld JJ, Kandel C, Biondi MJ, Kozak RA, Zahoor MA, Lemieux C, Borgia SM, Boggild AK, Powis J, McCready J, et al. 2021. Peginterferon lambda for the treatment of outpatients with COVID-19: a phase 2, placebo-controlled randomised trial. Lancet Respir Med 9:498–510. https://doi.org/10.1016/S2213-2600(20)30566-X

19. Flisiak R, Shiffman M, Arenas J, Cheinquer H, Nikitin I, Dong Y, Rana K, Srinivasan S. 2016. A randomized study of peginterferon lambda-1a compared to peginterferon Alfa-2a in combination with ribavirin and telaprevir in patients with genotype-1 chronic hepatitis C. PLoS One 11:e0164563. https://doi.org/10.1371/journal.pone.0164563

20. Muir AJ, Arora S, Everson G, Flisiak R, George J, Ghalib R, Gordon SC, Gray T, Greenbloom S, Hassanein T, et al. 2014. A randomized phase 2b study of peginterferon lambda-1a for the treatment of chronic HCV infection. J Hepatol 61:1238–1246. https://doi.org/10.1016/j.jhep.2014.07.022

21. Baldridge MT, Lee S, Brown JJ, McAllister N, Urbanek K, Dermody TS, Nice TJ, Virgin HW. 2017. Expression of *Ifnlr1* on intestinal epithelial cells is critical to the antiviral effects of interferon lambda against norovirus and reovirus. J Virol 91:e02079-16. https://doi.org/10.1128/JVI.02079-16

22. Casazza RL, Philip DT, Lazear HM. 2022. Interferon lambda signals in maternal tissues to exert protective and pathogenic effects in a gestational stage-dependent manner. mBio 13:e0385721. https://doi.org/10.1128/mbio.03857-21

23. Coldbeck-Shackley RC, Romeo O, Rosli S, Gearing LJ, Gould JA, Lim SS, Van der Hoek KH, Eyre NS, Shue B, Robertson SA, Best SM, Tate MD, Hertzog PJ, Beard MR. 2023. Constitutive expression and distinct properties of IFN-epsilon protect the female reproductive tract from Zika virus infection. PLoS Pathog 19:e1010843. https://doi.org/10.1371/journal.ppat.1010843

24. Zhou Z, Hamming OJ, Ank N, Paludan SR, Nielsen AL, Hartmann R. 2007. Type III interferon (IFN) induces a type I IFN-like response in a restricted subset of cells through signaling pathways involving both the JAK-STAT pathway and the mitogen-activated protein kinases. J Virol 81:7749–7758. https://doi.org/10.1128/JVI.02438-06

25. Caine EA, Scheaffer SM, Arora N, Zaitsev K, Artyomov MN, Coyne CB, Moley KH, Diamond MS. 2019. Interferon lambda protects the female reproductive tract against Zika virus infection. Nat Commun 10:280. https://doi.org/10.1038/s41467-018-07993-2

26. Galani IE, Triantafyllia V, Eleminiadou E-E, Koltsida O, Stavropoulos A, Manioudaki M, Thanos D, Doyle SE, Kotenko SV, Thanopoulou K, Andreakos E. 2017. Interferon-λ mediates non-redundant front-line antiviral protection against influenza virus infection without compromising host fitness. Immunity 46:875–890. https://doi.org/10.1016/j.immuni.2017.04.025

27. Good C, Wells AI, Coyne CB. 2019. Type III interferon signaling restricts enterovirus 71 infection of goblet cells. Sci Adv 5:eaau4255. https://doi.org/10.1126/sciadv.aau4255

28. Jagger BW, Miner JJ, Cao B, Arora N, Smith AM, Kovacs A, Mysorekar IU, Coyne CB, Diamond MS. 2017. Gestational stage and IFN-λ signaling regulate ZIKV infection in utero. Cell Host Microbe 22:366–376. https://doi.org/10.1016/j.chom.2017.08.012

29. Chami B, Yeung AWS, van Vreden C, King NJC, Bao S. 2014. The role of CXCR3 in DSS-induced colitis. PLoS One 9:e101622. https://doi.org/10.1371/journal.pone.0101622

30. Chami B, Yeung A, Buckland M, Liu H, M. Fong G, Tao K, Bao S. 2017. CXCR3 plays a critical role for host protection against salmonellosis. Sci Rep 7:10181. https://doi.org/10.1038/s41598-017-09150-z

31. Karin N. 2020. CXCR3 ligands in cancer and autoimmunity, chemoattraction of effector T cells, and beyond. Front Immunol 11:976. https://doi.org/10.3389/fimmu.2020.00976

32. Wojtasiak M, Pickett DL, Tate MD, Bedoui S, Job ER, Whitney PG, Brooks AG, Reading PC. 2010. Gr-1⁺ cells, but not neutrophils, limit virus replication and lesion development following flank infection of mice with herpes simplex virus type-1. Virology 407:143–151. https://doi.org/10.1016/j.virol.2010.08.001

33. Eichelberger KR, Jones GS, Goldman WE. 2019. Inhibition of neutrophil primary granule release during *Yersinia pestis* pulmonary infection. mBio 10:e02759-19. https://doi.org/10.1128/mBio.02759-19

34. Phillipson M, Heit B, Colarusso P, Liu L, Ballantyne CM, Kubes P. 2006. Intraluminal crawling of neutrophils to emigration sites: a molecularly distinct process from adhesion in the recruitment cascade. J Exp Med 203:2569–2575. https://doi.org/10.1084/jem.20060925

35. Zenaro E, Pietronigro E, Della Bianca V, Piacentino G, Marongiu L, Budui S, Turano E, Rossi B, Angiari S, Dusi S, Montresor A, Carlucci T, Nanì S, Tosadori G, Calciano L, Catalucci D, Berton G, Bonetti B, Constantin G. 2015. Neutrophils promote Alzheimer's disease-like pathology and cognitive decline via LFA-1 integrin. Nat Med 21:880–886. https://doi.org/10.1038/nm.3913

36. Broggi A, Tan Y, Granucci F, Zanoni I. 2017. IFN-λ suppresses intestinal inflammation by non-translational regulation of neutrophil function. Nat Immunol 18:1084–1093. https://doi.org/10.1038/ni.3821

37. Espinosa V, Dutta O, McElrath C, Du P, Chang Y-J, Cicciarelli B, Pitler A, Whitehead I, Obar JJ, Durbin JE, Kotenko SV, Rivera A. 2017. Type III interferon is a critical regulator of innate antifungal immunity. Sci Immunol 2:eaan5357. https://doi.org/10.1126/sciimmunol.aan5357

38. Boff D, Crijns H, Janssens R, Vanheule V, Menezes GB, Macari S, Silva TA, Amaral FA, Proost P. 2018. The chemokine fragment CXCL9(74-103) diminishes neutrophil recruitment and joint inflammation in antigen-induced arthritis. J Leukoc Biol 104:413–422. https://doi.org/10.1002/JLB.3MA1217-502R

39. Boff D, Russo RC, Crijns H, de Oliveira VLS, Mattos MS, Marques PE, Menezes GB, Vieira AT, Teixeira MM, Proost P, Amaral FA. 2022. The therapeutic treatment with the GAG-binding chemokine fragment CXCL9(74-103) attenuates neutrophilic inflammation and lung dysfunction during *Klebsiella pneumoniae* infection in mice. Int J Mol Sci 23:6246. https://doi.org/10.3390/ijms23116246

40. Hartl D, Krauss-Etschmann S, Koller B, Hordijk PL, Kuijpers TW, Hoffmann F, Hector A, Eber E, Marcos V, Bittmann I, Eickelberg O, Griese M, Roos D. 2008. Infiltrated neutrophils acquire novel chemokine receptor expression and chemokine responsiveness in chronic inflammatory lung diseases. J Immunol 181:8053–8067. https://doi.org/10.4049/jimmunol.181.11.8053

41. Forero A, Ozarkar S, Li H, Lee CH, Hemann EA, Nadjsombati MS, Hendricks MR, So L, Green R, Roy CN, Sarkar SN, von Moltke J, Anderson SK, Gale M Jr, Savan R. 2019. Differential activation of the transcription factor IRF1 underlies the distinct immune responses elicited by type I and type III Interferons. Immunity 51:451–464. https://doi.org/10.1016/j.immuni.2019.07.007

42. Hemann EA, Green R, Turnbull JB, Langlois RA, Savan R, Gale M. 2019. Interferon-λ modulates dendritic cells to facilitate T cell immunity during infection with influenza A virus. Nat Immunol 20:1035–1045. https://doi.org/10.1038/s41590-019-0408-z

43. Grau KR, Zhu S, Peterson ST, Helm EW, Philip D, Phillips M, Hernandez A, Turula H, Frasse P, Graziano VR, Wilen CB, Wobus CE, Baldridge MT, Karst SM. 2020. The intestinal regionalization of acute norovirus infection is regulated by the microbiota via bile acid-mediated priming of type III interferon. Nat Microbiol 5:84–92. https://doi.org/10.1038/s41564-019-0602-7

44. Ingle H, Makimaa H, Aggarwal S, Deng H, Foster L, Li Y, Kennedy EA, Peterson ST, Wilen CB, Lee S, Suthar MS, Baldridge MT. 2023. IFN-λ derived from nonsusceptible enterocytes acts on tuft cells to limit persistent norovirus. Sci Adv 9:eadi2562. https://doi.org/10.1126/sciadv.adi2562

45. Ye L, Schnepf D, Becker J, Ebert K, Tanriver Y, Bernasconi V, Gad HH, Hartmann R, Lycke N, Staeheli P. 2019. Interferon-λ enhances adaptive mucosal immunity by boosting release of thymic stromal lymphopoietin. Nat Immunol 20:593–601. https://doi.org/10.1038/s41590-019-0345-x

46. Douam F, Soto Albrecht YE, Hrebikova G, Sadimin E, Davidson C, Kotenko SV, Ploss A. 2017. Type III interferon-mediated signaling is critical for controlling live attenuated yellow fever virus infection *in vivo*. mBio 8:e00819-17. https://doi.org/10.1128/mBio.00819-17

47. Lazear HM, Daniels BP, Pinto AK, Huang AC, Vick SC, Doyle SE, Gale M, Klein RS, Diamond MS. 2015. Interferon-λ restricts West Nile virus neuroinvasion by tightening the blood-brain barrier. Sci Transl Med 7:284ra59. https://doi.org/10.1126/scitranslmed.aaa4304

48. Goel RR, Wang X, O'Neil LJ, Nakabo S, Hasneen K, Gupta S, Wigerblad G, Blanco LP, Kopp JB, Morasso MI, Kotenko SV, Yu Z-X, Carmona-Rivera C, Kaplan MJ. 2020. Interferon lambda promotes immune dysregulation

and tissue inflammation in TLR7-induced lupus. Proc Natl Acad Sci U S A 117:5409–5419. https://doi.org/10.1073/pnas.1916897117

49. Santer DM, Minty GES, Golec DP, Lu J, May J, Namdar A, Shah J, Elahi S, Proud D, Joyce M, Tyrrell DL, Houghton M. 2020. Differential expression of interferon-lambda receptor 1 splice variants determines the magnitude of the antiviral response induced by interferon-lambda 3 in human immune cells. PLoS Pathog 16:e1008515. https://doi.org/10.1371/journal.ppat.1008515

50. Hor JL, Heath WR, Mueller SN. 2017. Neutrophils are dispensable in the modulation of T cell immunity against cutaneous HSV-1 infection. Sci Rep 7:41091. https://doi.org/10.1038/srep41091

51. Ank N, Iversen MB, Bartholdy C, Staeheli P, Hartmann R, Jensen UB, Dagnaes-Hansen F, Thomsen AR, Chen Z, Haugen H, Klucher K, Paludan SR. 2008. An important role for type III interferon (IFN-Lambda/IL-28) in TLR-induced antiviral activity. J Immunol 180:2474–2485. https://doi.org/10.4049/jimmunol.180.4.2474

52. Lebratti T, Lim YS, Cofie A, Andhey P, Jiang X, Scott J, Fabbrizi MR, Ozantürk AN, Pham C, Clemens R, Artyomov M, Dinauer M, Shin H. 2021. A sustained type I IFN-neutrophil-IL-18 axis drives pathology during mucosal viral infection. Elife 10:e65762. https://doi.org/10.7554/eLife.65762

53. Lopez CA, Dulson SJ, Lazear HM. 2022. Zika virus replicates in the vagina of mice with intact interferon signaling. J Virol 96:e0121922. https://doi.org/10.1128/jvi.01219-22

54. Wollenberg A, Wetzel S, Burgdorf WHC, Haas J. 2003. Viral infections in atopic dermatitis: pathogenic aspects and clinical management. J Allergy Clin Immunol 112:667–674. https://doi.org/10.1016/j.jaci.2003.07.001

55. Wolk K, Witte K, Witte E, Raftery M, Kokolakis G, Philipp S, Schönrich G, Warszawska K, Kirsch S, Prösch S, Sterry W, Volk H-D, Sabat R. 2013. IL-29 is produced by T(H)17 cells and mediates the cutaneous antiviral competence in psoriasis. Sci Transl Med 5:204ra129. https://doi.org/10.1126/scitranslmed.3006245

56. Kawakami Y, Ando T, Lee J-R, Kim G, Kawakami Y, Nakasaki T, Nakasaki M, Matsumoto K, Choi YS, Kawakami T. 2017. Defective natural killer cell activity in a mouse model of eczema herpeticum. J Allergy Clin Immunol 139:997–1006. https://doi.org/10.1016/j.jaci.2016.06.034

57. Reed JL, Scott DE, Bray M. 2012. Eczema Vaccinatum. Clin Infect Dis 54:832–840. https://doi.org/10.1093/cid/cir952

58. Wharton M, Strikas RA, Harpaz R, Rotz LD, Schwartz B, Casey CG, Pearson ML, Anderson LJ, Advisory Committee on Immunization Practices, Healthcare Infection Control Practices Advisory Committee. 2003. Recommendations for using smallpox vaccine in a pre-event vaccination program. Supplemental recommendations of the advisory committee on immunization practices (ACIP) and the healthcare infection control practices advisory committee (HICPAC). MMWR Recomm Rep 52:1–16.

59. Novais FO, Amorim CF, Scott P. 2021. Host-directed therapies for cutaneous leishmaniasis. Front Immunol 12:660183. https://doi.org/10.3389/fimmu.2021.660183

60. Shmeleva EV, Gomez de Agüero M, Wagner J, Enright AJ, Macpherson AJ, Ferguson BJ, Smith GL. 2022. Smallpox vaccination induces a substantial increase in commensal skin bacteria that promote pathology and influence the host response. PLoS Pathog 18:e1009854. https://doi.org/10.1371/journal.ppat.1009854

61. Miner JJ, Platt DJ, Ghaznavi CM, Chandra P, Santeford A, Menos AM, Dong Z, Wang ER, Qian W, Karozichian ES, Philips JA, Apte RS. 2020. HSV-1 and Zika virus but not SARS-CoV-2 replicate in the human cornea and are restricted by corneal type III interferon. Cell Rep 33:108339. https://doi.org/10.1016/j.celrep.2020.108339

62. Friedman HM, Macarak EJ, MacGregor RR, Wolfe J, Kefalides NA. 1981. Virus infection of endothelial cells. J Infect Dis 143:266–273. https://doi.org/10.1093/infdis/143.2.266

63. Ma JZ, Russell TA, Spelman T, Carbone FR, Tscharke DC. 2014. Lytic gene expression is frequent in HSV-1 latent infection and correlates with the engagement of a cell-intrinsic transcriptional response. PLoS Pathog 10:e1004237. https://doi.org/10.1371/journal.ppat.1004237

64. Lou F, Sun Y, Wang H. 2020. Protocol for flow cytometric detection of immune cell infiltration in the epidermis and dermis of a psoriasis mouse model. STAR Protoc 1:100115. https://doi.org/10.1016/j.xpro.2020.100115

65. Sakamoto K, Goel S, Funakoshi A, Honda T, Nagao K. 2022. Flow cytometry analysis of the subpopulations of mouse keratinocytes and skin immune cells. STAR Protoc 3:101052. https://doi.org/10.1016/j.xpro.2021.101052

66. Li F, Adase CA, Zhang L-J. 2017. Isolation and culture of primary mouse keratinocytes from neonatal and adult mouse skin. J Vis Exp 56027:56027. https://doi.org/10.3791/56027